












REVIEW ARTICLE | NOVEMBER 25 2025

## Organic active waveguides

Do Wan Kim ; Seokho Kim ; Jinho Choi ; Jaehyun Lee ; Yongmin Baek ; Kyusang Lee  ;  
Dong Hyuk Park  ; Jongchan Kim  



*Appl. Phys. Rev.* 12, 041321 (2025)

<https://doi.org/10.1063/5.0276463>



## Special Topics Open for Submissions

[Learn More](#)

# Organic active waveguides

Cite as: Appl. Phys. Rev. **12**, 041321 (2025); doi: 10.1063/5.0276463  
Submitted: 18 April 2025 · Accepted: 5 November 2025 ·  
Published Online: 25 November 2025



Do Wan Kim,<sup>1</sup>  Seokho Kim,<sup>1,2</sup>  Jinho Choi,<sup>3,4</sup>  Jaehyun Lee,<sup>5</sup>  Yongmin Baek,<sup>1,6</sup>  Kyusang Lee,<sup>1,7,a)</sup>   
Dong Hyuk Park,<sup>3,8,a)</sup>  and Jongchan Kim<sup>5,9,a)</sup> 

## AFFILIATIONS

- <sup>1</sup>Department of Electrical and Computer Engineering, University of Virginia, Charlottesville, Virginia 22904, USA  
<sup>2</sup>Department of Chemical and Biological Engineering, Korea University, Seoul 02841, Republic of Korea  
<sup>3</sup>Department of Chemical Engineering, Inha University, Incheon 22212, Republic of Korea  
<sup>4</sup>Department of Materials Science and Engineering, University of Michigan, Ann Arbor, Michigan 48109, USA  
<sup>5</sup>Department of Integrated Display Engineering, Yonsei University, Seoul 03722, Republic of Korea  
<sup>6</sup>Department of Mechanical Engineering, Seoul National University, Seoul 08826, Republic of Korea  
<sup>7</sup>Department of Materials Science and Engineering, University of Virginia, Charlottesville, Virginia 22904, USA  
<sup>8</sup>Program in Biomedical Science & Engineering, Inha University, Incheon 22212, Republic of Korea  
<sup>9</sup>Department of Electrical and Electronic Engineering, Yonsei University, Seoul 03722, Republic of Korea

<sup>a)</sup>Authors to whom correspondence should be addressed: [kyusang@virginia.edu](mailto:kyusang@virginia.edu); [donghyuk@inha.ac.kr](mailto:donghyuk@inha.ac.kr); and [jck@yonsei.ac.kr](mailto:jck@yonsei.ac.kr)

## ABSTRACT

As the demand for high bandwidth and long-distance data transmission escalates in modern computing, optical interconnects via waveguides have attracted significant attention. While conventional inorganic materials-based waveguide necessitates complex components such as grating couplers and optical amplifiers, organic semiconductor-based waveguides offer simplified systems with unique functionalities stemming from their inherent radiative properties that facilitate efficient light–matter interactions, such as exciton–polariton formation and Förster resonance energy transfer. These interactions enable active light modulation, encompassing intensity control, wavelength shift, exciton–polariton lasing, and nonlinear optical effects. Moreover, their optical properties and structural geometries can be precisely tuned through molecular design and controlled synthesis techniques. As a result, organic waveguides have been explored for a range of applications including optical-logic operations, bio-chemical sensing, and advanced photonic integration systems. In this review, we delineate the fundamental principles of organic semiconductor waveguides, as well as their fabrication and potential impact on various photonic applications.

Published under an exclusive license by AIP Publishing. <https://doi.org/10.1063/5.0276463>

## TABLE OF CONTENTS

I. INTRODUCTION.....	1
II. PRINCIPLES OF ORGANIC ACTIVE WAVEGUIDES.....	3
A. Light propagation in active waveguides.....	4
B. Optical losses in active waveguides.....	5
C. Advanced functions in active waveguides.....	6
III. STRUCTURAL DESIGN STRATEGY FOR ACTIVE WAVEGUIDES.....	6
A. Molecular design.....	6
B. Structural design.....	8
C. Fabrication and integration.....	10
IV. APPLICATION OF ACTIVE WAVEGUIDE USING ORGANIC SEMICONDUCTORS.....	11
A. Optical sensors.....	11
B. Lasing.....	13

C. Optical signal manipulation.....	13
V. CONCLUSION AND PERSPECTIVES.....	15

## I. INTRODUCTION

In 1997, when optically pumped laser emission was first achieved in thin films of organic molecules configured as two-dimensional (2D) planar waveguides.<sup>1</sup> This seminal breakthrough was soon followed by the discovery of optical waveguiding properties in nanometer-scale organic fibers.<sup>2</sup> Early investigations focused intensively on enhancing waveguide performance through precise molecular and geometrical design with particular emphasis on minimizing optical loss, for instance, by engineering hollow tubular structures that enhance optical confinement.<sup>3</sup> More recent studies broadened the functional scope of these devices; for instance, the excitonic properties of organic materials

have been employed to develop optical regulators that convert various input wavelengths into white light or modulate intensity under external electric fields.<sup>4,5</sup> Additionally, heterostructure engineering has been employed to realize logic gates,<sup>6</sup> multichannel operations,<sup>7</sup> and bio-sensing applications,<sup>8</sup> and electrically conducting waveguides.<sup>9</sup> Advances in controlling intermolecular interactions have further allowed for the modulation of structural properties, thereby enhancing flexibility and facilitating the seamless integration of waveguide segments.<sup>10–12</sup> More recently, pseudo-plastic organic crystals have been employed to realize hierarchical waveguide networks capable of mimicking neural-like signal flow, expanding the functional versatility of organic photonic systems.<sup>13</sup>

Despite these advancements in performance and functionality, organic waveguides encounter critical challenges that need to be overcome for their widespread practical and commercial applications. Organic waveguides often suffer from limited scalability, narrower bandwidth, and reduced long-term operational stability.<sup>14,15</sup> Moreover, the inherent thermal and mechanical vulnerabilities of organic semiconductors further complicate their integration into photonic circuits. In contrast, mature inorganic platforms such as silicon nitride (Si<sub>3</sub>N<sub>4</sub>) waveguides offer relatively robust thermal stability, broad transparency windows, and complementary metal-

oxide-semiconductor (CMOS)-compatible processing, as shown in Table I, delivering a comparative summary of key parameters between organic and Si<sub>3</sub>N<sub>4</sub>-based waveguides, highlighting the complementary advantages and fundamental tradeoffs associated with each system.

However, organic materials exhibit a unique characteristic: strong exciton-mediated light-matter interactions. This property enables realizing active waveguides, which provide distinct advantages over inorganic counterparts, and are emerging as a promising platform in various aspects.<sup>16–20</sup> The active waveguides are defined as structures in which the guiding medium itself functions as an emissive or energy-transferring component, thereby enabling amplification, modulation, and nonlinear optical responses. These features are attributed to the high exciton binding energies of organic materials, which impart a strong radiative nature,<sup>21–24</sup> enabling them to act not only as conduits but also as active media for generating tunable and coherent light, which is an essential capability for optical communication, sensing, and integrated photonic circuits.<sup>2,25–27</sup> To optimize performance, molecular design strategies have been developed to improve radiative efficiency and tailor absorption and emission spectra, while engineering of molecular packing and waveguide architectures has enhanced optical confinement and reduced propagation losses.<sup>28–32</sup> These

**TABLE I.** Comparison of key characteristics between typical organic waveguides and representative inorganic counterparts (e.g., Si<sub>3</sub>N<sub>4</sub>-based waveguides). Parameters include refractive index, loss coefficient, transparency range, thermal and mechanical stability, thermo-optic coefficient, bending radius, fabrication requirements, integration compatibility, and functional capabilities. While Si<sub>3</sub>N<sub>4</sub> waveguides offer superior stability and ultra-low optical losses, organic waveguides provide distinct advantages in flexibility, integration with soft substrates, and active photonic functionalities under moderate fabrication conditions.

	Typical organic waveguides	Ref.	Inorganic Si3N4-based waveguides	Ref.
Refractive index	1.4–2.0 ( $n_g \sim 10$ )	32, 172	$\sim 2.0$ ( $n_g \sim 2$ )	173, 174
Loss coefficient	Low over short distances (0.00027–1 dB/ $\mu$ m)	32, 166	Extremely low over long distances (1–10 dB/m)	168, 169
Transparency range	Visible to NIR (400 nm–1.6 $\mu$ m)	14, 141, 175	Visible to MIR (400 nm–6.7 $\mu$ m)	169, 176
Thermal stability	Moderate/Low: Degradation or deformation in 100–250 °C range	177, 178	High: Needs high temperature (850 °C) to deform, and devices are stable up to $\sim 100$ °C.	179, 180
Thermo-optic coefficient	Moderate ( $1.8 \times 10^{-4}/^{\circ}\text{C}$ )	181	Low ( $1.7 \times 10^{-5}/^{\circ}\text{C}$ )	181
Mechanical properties	Flexible. Degrade over time	184, 182	Rigid and brittle. Extremely stable over time.	174
Bending radius	$\sim$ Tens of $\mu$ m	182	$\sim$ Hundreds of $\mu$ m	174, 183, 169
Fabrication	Low cost, scalable, moderate fabrication environment	61	High precision, CMOS-fab compatible, harsh fabrication environment (high temperature and vacuum)	168
Integration compatibility	Compatible with organic light sources and flexible substrate	153	CMOS monolithic integration possible, but post-CMOS integration limited due to high annealing temperature ( $>850$ °C)	184
Functionality/application field	Active; bio-sensing, light modulation, 2.5/3D integration	153, 126, 185	Passive; Supports nonlinear optics, supercontinuum, Kerr combs	184, 186, 187

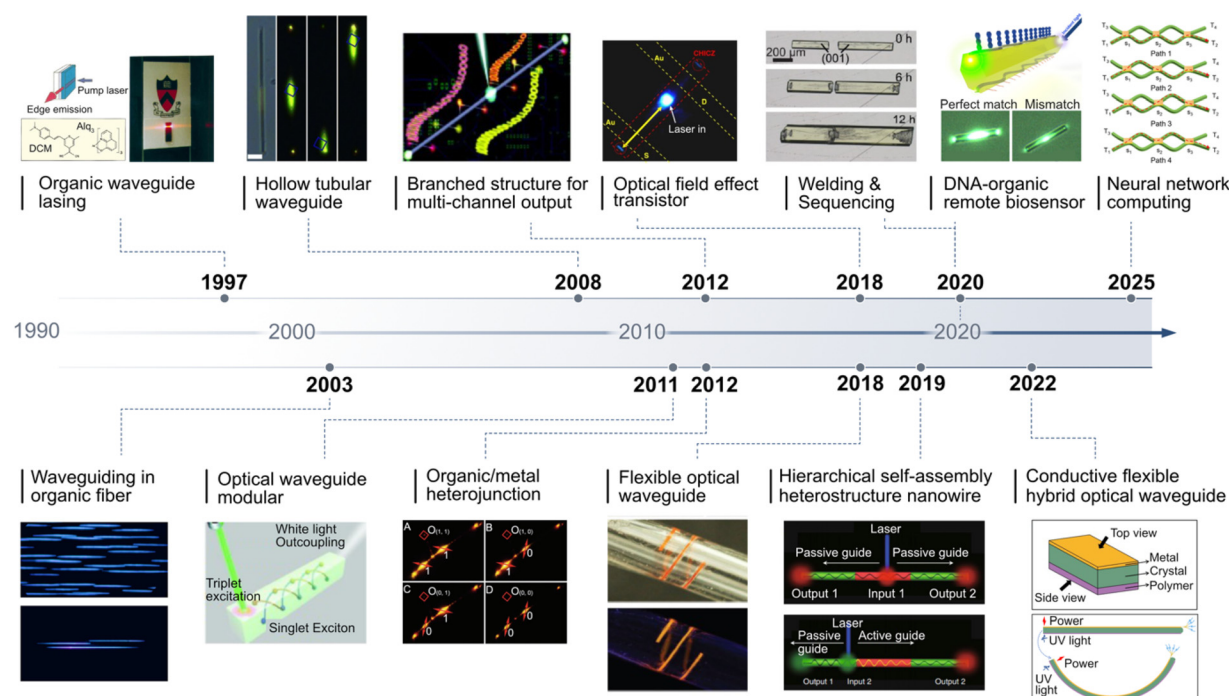


**FIG. 1.** Timeline infographic that delineates the seminal milestones in the evolution of organic waveguide technology.<sup>1–7,9–12</sup> Reproduced with permission from Kozlov *et al.*, *Nature* **389**, 362 (1997). Copyright 1997 Springer Nature. Reproduced with permission from Balzer *et al.*, *Phys. Rev. B* **67**, 115408 (2003). Copyright 2003 American Physical Society. Reproduced with permission from Zhao *et al.*, *Angew. Chem. Int. Ed.* **47**, 7301 (2008). Copyright 2008 John Wiley and Sons. Reproduced with permission from Zhang *et al.*, *Adv. Mater.* **23**, 1380 (2011). Copyright 2011 John Wiley and Sons. Reproduced with permission from Zhao *et al.*, *Nat. Commun.* **9**, 4790 (2018). Copyright 2018 Author(s), licensed under a Creative Commons Attribution (CC BY) license. Reproduced with permission from Yan *et al.*, *Adv. Mater.* **24**, 5681 (2012). Copyright 2012 John Wiley and Sons. Reproduced with permission from Zheng *et al.*, *J. Am. Chem. Soc.* **134**, 2880 (2012). Copyright 2012 American Chemical Society. Reproduced with permission from Yang *et al.*, *Nat. Commun.* **13**, 7874 (2022). Copyright 2022 Author(s), licensed under a Creative Commons Attribution (CC BY) license. Reproduced with permission from Huang *et al.*, *Adv. Mater.* **30**, 1800814 (2018). Copyright 2018 John Wiley and Sons. Reproduced with permission from Zhuo *et al.*, *Nat. Commun.* **10**, 3839 (2019). Copyright 2019 Author(s), licensed under a Creative Commons Attribution (CC BY) license. Copyright 2019 Springer Nature. Reproduced with permission from Catalano *et al.*, *Adv. Funct. Mater.* **30**, 2003443 (2020). Copyright 2020 John Wiley and Sons. Reproduced with permission from Kumar *et al.*, *Angew. Chem. Int. Ed.* **64**, e202502122 (2025). Copyright 2025 John Wiley and Sons.

advances have expanded the scope of organic waveguides across diverse photonic systems, as summarized in Fig. 1.<sup>33–36</sup>

Several reviews have provided valuable insights into the structural design, material classes, and mechanical flexibility of organic waveguides, and others have highlighted low-dimensional heterostructures and their photonic properties.<sup>31,32,37–41</sup> However, comparatively less attention has been directed toward active optical modulation, nonlinear photonic behaviors driven by exciton–photon interactions, and system-level integration into logic circuits, optical computing, or neuromorphic platforms.<sup>31,32,37–41</sup>

In this review, we place particular emphasis on exciton-mediated mechanisms as the foundation for dynamic modulation in organic active waveguides. This review outlines the fundamental principles governing light propagation and loss in active organic waveguides, examines structural and molecular design strategies that enable precise control over their photonic behavior, and survey recent advances in their integration across applications ranging from lasing and optical logic to biosensing. Beyond consolidating these developments, we provide insights into how excitonic interactions, heterostructure engineering, and novel fabrication approaches collectively expand the functional landscape of organic photonics. Finally, we highlight the

remaining challenges, such as scalable crystal growth, operational stability, and device-level integration, and discuss future opportunities where organic active waveguides may play a pivotal role in next-generation photonic technologies, including neuromorphic computing and biocompatible optical interfaces.

## II. PRINCIPLES OF ORGANIC ACTIVE WAVEGUIDES

Both passive and active organic waveguides operate based on the spatial confinement of the optical field within a guiding medium, achieved through refractive index engineering. Typically, the core material possesses a refractive index higher than that of the surrounding cladding, enabling total internal reflection (TIR). This occurs when the incident angle within the core exceeds the critical angle  $\theta_C = \arcsin(\frac{n_0}{n})$ , where  $n_0$  and  $n$  are the refractive indices of the cladding and core, respectively. Consequently, the optical field remains confined within the core and propagates along the waveguide structure.<sup>14,15,31,42</sup>

Despite their structural similarities, passive and active waveguides differ fundamentally in function. Passive waveguides solely transmit externally introduced light with minimal loss, functioning as optical conduits or spectral filters.<sup>14,43–45</sup> In such systems, guided propagation

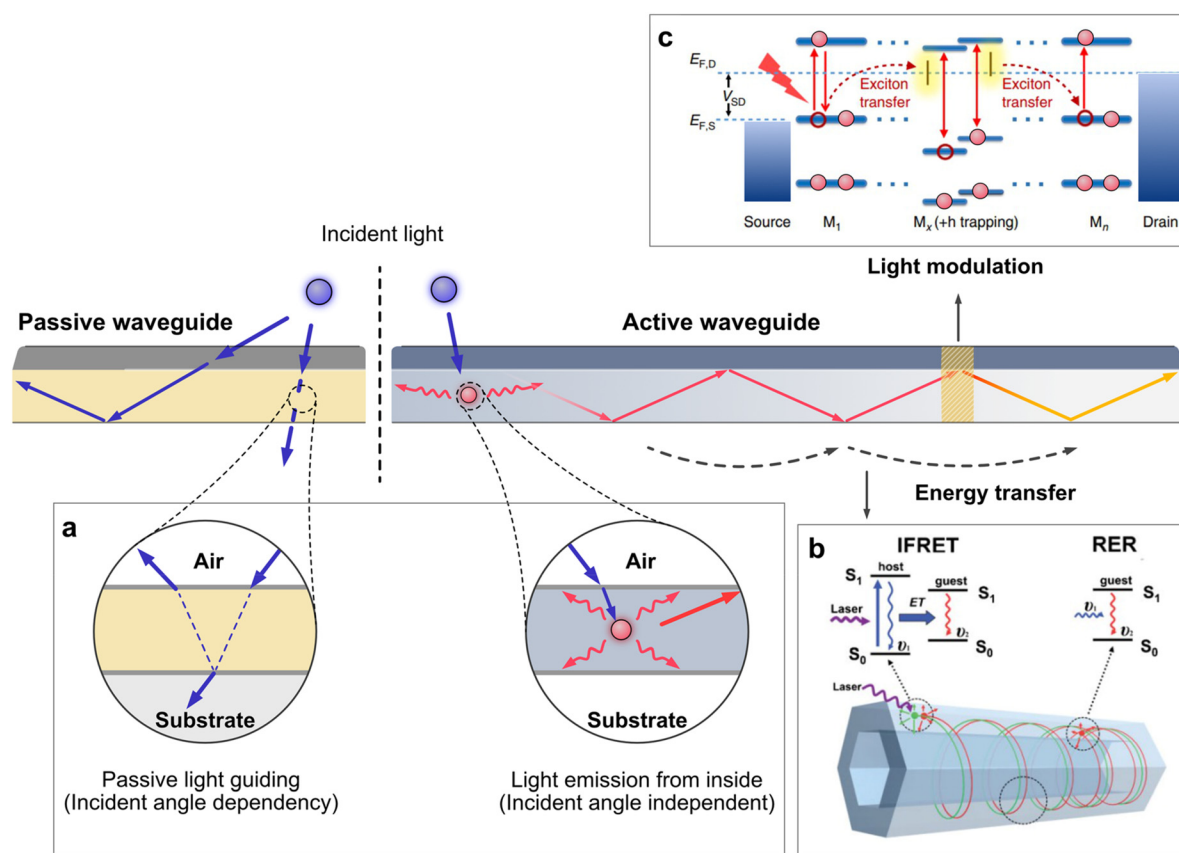


**FIG. 2.** Principle of wave propagation and optical losses in organic waveguides. (a) Conceptual illustration comparing the characteristics and functions of passive and active organic waveguides. Strong dependence of light guiding on incident angle and interface conditions in the passive section. (b) Schematic of the annular cavity within a binary microtube and the corresponding energy diagrams that detail the intermolecular Förster resonance energy transfer (IFRET) and remote energy relay (RER) processes.<sup>16</sup> Reproduced with permission from Liao *et al.*, *Adv. Mater.* **21**, 4153 (2009). Copyright 2009 John Wiley and Sons. (c) Schematic illustration of the suppression of resonant energy transfer among photo-generated excitons due to an energy gap mismatch between neighboring molecules (M<sub>1</sub>, M<sub>x</sub>, and M<sub>n</sub>) in an organic crystal, induced by hole trapping under external voltage control.<sup>5</sup> Reproduced with permission from Zhao *et al.*, *Nat. Commun.* **9**, 4790 (2018). Copyright 2018 Author(s), licensed under a Creative Commons Attribution (CC BY) license.

strictly depends on geometric coupling conditions, particularly the incident angle of the light.

In contrast, active organic waveguides incorporate an emissive or energy-transferring medium as the core material itself. Here, the optical processes intrinsic to the material such as absorption, emission, and excitonic energy transfer play a critical role in its operation (Fig. 2).<sup>3,18,46,47</sup>

### A. Light propagation in active waveguides

In active waveguides, light propagation does not solely rely on geometric coupling. Instead, excitons generated within the core recombine radiatively, emitting photons that are subsequently reabsorbed by adjacent molecules. This process facilitates light guiding even in the absence of strict geometric incident-angle conditions. The efficiency of these interactions depends on intrinsic properties of the core materials such as energy gap, radiative recombination rate, and energy transfer efficiency. In strongly confined structures, these excitonic interactions give rise to quasi-particles known as exciton-polaritons (EPs), which

offer unique dispersion characteristics and enhanced guiding performance.<sup>22,23,48</sup>

EPs inherit the light effective mass and coherence properties of photons while retaining the strong nonlinearity and interaction strength of excitons, thereby combining the advantages of both matter and light. They enable efficient light transport in active organic waveguides through repeated absorption-emission cycles, thereby decoupling propagation from strict geometric input conditions. This exciton-mediated mechanism significantly relaxes constraints on input beam alignment, enabling flexible excitation schemes and maintaining efficient light guiding even under non-directional or diffuse illumination.

A defining advantage of organic materials is their ability to support stable EP formation at room temperature due to high exciton binding energies and strong light-matter interactions.<sup>22–24</sup> The strong coupling between cavity photons and Frenkel excitons results in quasi-particles with significantly reduced group velocities, typically on the order of  $10^7 \text{ m s}^{-1}$ , compared to that of uncoupled photons.<sup>49,50</sup> The reduced velocity corresponds to a markedly high group refractive



index ( $n_g > 10$ ) near excitonic resonances, as revealed by Fabry–Pérot mode analyses in single organic dye nanofibers.<sup>22,51</sup> These high group refractive indices compress the polaritonic wavelength, allowing EP modes to propagate in nanostructures with dimensions well below the diffraction limit. The resulting strong spatial confinement reduces radiation losses and supports effective polaritonic guiding, even in bent or subwavelength scale configurations.<sup>25,52–54</sup> Moreover, the dispersive nature of EPs allows dynamic spectral and spatial modulation, providing a versatile platform for low-threshold lasing, energy transport, and nonlinear optical functionalities.

To stabilize and enhance EPs propagation, material systems must exhibit high exciton binding energies, strong  $\pi$ - $\pi$  interactions, and well-defined photonic cavity architectures.<sup>55</sup> Accordingly, strategies aimed at optimizing molecular packing to minimize intermolecular distances and strengthen  $\pi$ - $\pi$  interactions are actively pursued to improve light-matter coupling and facilitate efficient EP propagation.<sup>56</sup>

While EPs provide coherent and long-range light transport, additional excitonic mechanisms such as Förster resonance energy transfer (FRET) and remote energy relay (RER) govern short-range wavelength-selective guidance and long-distance propagation in active organic waveguides.<sup>57,58</sup> At the nanoscale, energy transfer via non-radiative dipole-dipole interactions, known as FRET, plays a crucial role in active organic waveguides,<sup>57</sup> enabling efficient exciton migration and short-range propagation through bandgap alignment between donor and acceptor species.<sup>52,59</sup> Beyond this short-range interaction, RER, where emitted photons are reabsorbed and re-emitted by

spatially separated molecules, enables energy transport well beyond the FRET range [Fig. 2(b)].<sup>16</sup> Taken together, EPs, FRET, and RER represent the fundamental mechanisms of active organic waveguides, enabling light propagation that is coherent, long ranged, and dynamically controllable through intrinsic excitonic interactions.

## B. Optical losses in active waveguides

In waveguide systems, optical losses are unavoidable, primarily arising from radiation leakage at waveguide boundaries (e.g., edges, bends, and discontinuities) and scattering caused by structural defects. When extended to active organic waveguides, these general mechanisms are accompanied by additional loss channels associated with excitonic processes (Fig. 3).<sup>60–62</sup> A prominent example is self-absorption, wherein organic materials absorb light within their excitonic transition range, which constitutes a significant loss channel. This loss becomes pronounced in systems with strong excitonic interactions, such as densely packed molecular assemblies, and is further intensified when emission and absorption bands exhibit significant spectral overlap.<sup>63</sup> In addition, exciton-exciton annihilation at high excitation densities introduces non-radiative decay pathways, limiting the achievable propagation length.<sup>64,65</sup> Furthermore, exciton dephasing and non-radiative recombination serve as intrinsic dissipative channels that weaken coherent EP transport.

To mitigate these exciton-related losses, various molecular design approaches have been widely employed. For instance, incorporation of donor-acceptor molecular systems with large Stokes shifts effectively

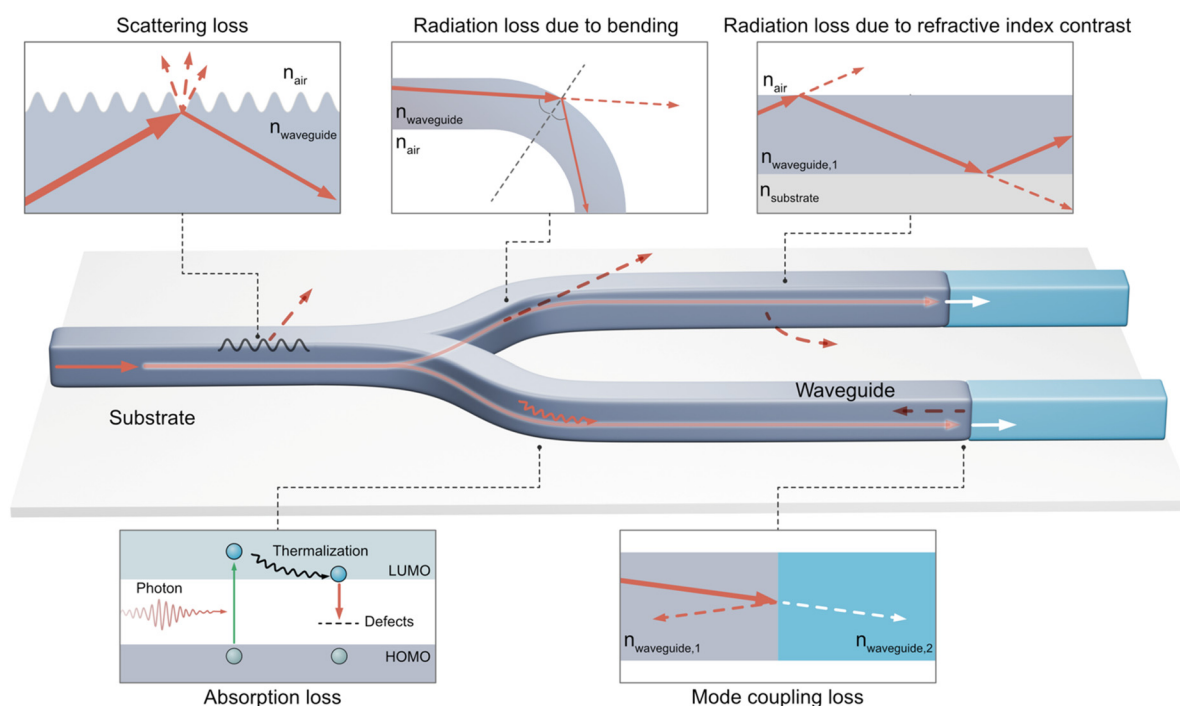


**FIG. 3.** Diagram outlining wave propagation in the organic waveguide, with an emphasis on the principal mechanisms responsible for optical losses. Structural mechanisms such as surface scattering, radiation at bends, and leakage due to modest refractive index contrast dominate in passive systems, while mode coupling at interfaces further degrades propagation efficiency. In active organic, waveguides experience additional dissipation channels associated with excitonic processes, including self-absorption caused by spectral overlap between emission and absorption bands, exciton-exciton annihilation at high excitation densities, and exciton dephasing or non-radiative recombination.

suppresses self-absorption by minimizing spectral overlap between emission and absorption bands.<sup>63,66</sup> Enhancing radiative quantum yield further reduces non-radiative decay.<sup>10,67</sup> In particular, engineering strong  $\pi$ - $\pi$  interactions facilitates the stabilization of excitonic states, thereby enabling stable EP formation at room temperature, which requires exciton binding energies and longitudinal-transverse splitting that exceed the thermal energy ( $kT_R \sim 25$  meV).<sup>22,68</sup> Moreover, considerable efforts have been devoted to designing high-quality cavities, achieving quality factors (Q-factors) in the range of 130 and 170,<sup>37,69</sup> which effectively suppress dissipative losses and support stable EP propagation.

In addition to this intrinsic dissipation, structural loss mechanisms further impede light propagation. For instance, radiation loss caused by the modest refractive index contrast between the waveguide core and cladding accounts for a major source of attenuation, particularly at the curvature. Scattering losses, often originating from structural inhomogeneities or surface roughness introduced during crystal growth or processing, also contribute to overall attenuation. Moreover, undesired mode coupling at interfaces or other imperfections can induce energy leakage into non-guided or radiative modes, further degrading propagation efficiency. Advanced molecular design approaches, such as tuning the electronic band structure and incorporating hybrid organic-inorganic components, have been employed to engineer the optical performance of organic semiconductor waveguides.

### C. Advanced functions in active waveguides

Active waveguides with subwavelength-width dimensions provide a suitable environment for confining both excitons and photons, thereby promoting the formation of EPs. Various organic materials support tightly bound Frenkel excitons characterized by strong binding energies of approximately 0.5–1 eV, showing strong longitudinal-transverse exciton splitting energy of approximately 1 eV and significant oscillator strengths, which together yield extended temporal and spatial coherence.<sup>22,23,70</sup> The exceptionally low effective mass of EPs facilitates Bose-Einstein condensation (BEC) at temperatures on the order of several hundred kelvin, resulting in unique features, such as polariton lasing and superfluidity.<sup>69,71–73</sup> These properties enable functionalities such as low-threshold coherent emission and enhanced light-matter interactions within organic waveguides. Importantly, recent studies have demonstrated that exciton-polaritons sustain coherent transport over tens to hundreds of micrometers, even in disordered or patterned dielectric environments, indicating their robustness against scattering and their compatibility with inorganic photonic platforms for polaritonic integrated circuits.<sup>50,74</sup>

Active waveguides utilize FRET to achieve effective wavelength tuning. By aligning donor and acceptor energy gaps, emission spectra can be engineered to span a broad spectral range.<sup>52,59</sup> For instance, in a hybrid system comprising 2,4,5-triphenylimidazole (TPI) and perylene microtubes [Fig. 2(c)], green emission is initially generated by FRET between closely associated TPI and perylene molecules. This short-range transfer is further extended through RER, wherein photons emitted by TPI are reabsorbed and re-emitted by spatially distributed perylene molecules, enabling energy transport over distances exceeding 100  $\mu\text{m}$  along the waveguide.<sup>16</sup> Moreover, the intensity of the guided light can be tuned by applying an external electric field. The applied field adjusts the exciton transfer rate by inducing hole trapping at

specific molecular sites, achieved by shifting orbital energy levels relative to neighboring molecules and disrupting the alignment required for resonant transfer [Fig. 2(d)]. Such control provides a pathway for electrically addressable modulation of guided light intensity.<sup>5</sup>

In addition, nonlinear optical phenomena have been realized in active organic waveguides, including multiphoton excitation and second-harmonic generation (SHG).<sup>75,76</sup> These effects can be enhanced by tailoring waveguide geometry, such as film thickness and molecular alignment. Additionally, molecular design strategies such as incorporating chiral architectures are utilized. Chiral molecular architectures foster non-centrosymmetric crystal packing, thereby increasing net polarization and SHG efficiency. Likewise, the push-pull electronic structure facilitates strong intramolecular charge transfer (CT), increasing molecular dipole moments and nonlinear polarizabilities, ultimately improving SHG efficiency. Together, these design strategies of organic waveguides significantly improve active manipulation of light.

In summary, active organic waveguides serve as versatile platforms where polaritonic condensation, long-range exciton-mediated transport, and nonlinear optical processes can be integrated. Their multifunctional nature enables versatile adaptability of organic active waveguides into a broad range of photonic applications.

## III. STRUCTURAL DESIGN STRATEGY FOR ACTIVE WAVEGUIDES

### A. Molecular design

The performance of active waveguides is fundamentally governed by the radiative characteristics of their constituent molecules, which are determined by both intrinsic photophysical properties and the morphological arrangement.<sup>77,78</sup> At the molecular level, the properties of these systems are closely linked to the conjugation length of the  $\pi$ -electron system; an increased conjugation length narrows the highest occupied molecular orbital (HOMO)-lowest unoccupied molecular orbital (LUMO) gap, inducing a redshift in the emission. The increased conjugation length also suppresses non-radiative decay by reducing the Franck-Condon overlap and minimizing internal conversion pathways.

Incorporating both electron-withdrawing groups (EWGs) and electron-donating groups (EDGs) within the molecular framework alters the electron density distribution of the  $\pi$ -conjugated structure, thereby tuning electron transitions and exciton dynamics.<sup>79,80</sup> For instance, a benzene derivative that combines symmetrical hydroxyl (EDG) and carbonyl (EWG) showed enhanced fluorescence efficiency and improved crystallinity. This enhancement arises from increased electron delocalization and substituents stabilization within the aromatic plane, facilitated by intermolecular hydrogen bonding [Fig. 4(a)].<sup>81</sup> In contrast to twisted or non-coplanar structures that promote non-radiative relaxation through internal conversion, a planar molecular conformation minimizes structural distortion in the excited state, thereby favoring radiative decay pathways. Symmetrically arranged EWG and EDG groups on the benzene rings exhibit stable, strong emission in solution as well as in amorphous films and densely packed crystal structures, with slightly red-shifted emission caused by aggregation. This behavior indicates an effective suppression of non-radiative decay processes that are typically observed in organic crystal due to strong  $\pi$ - $\pi$  interactions.

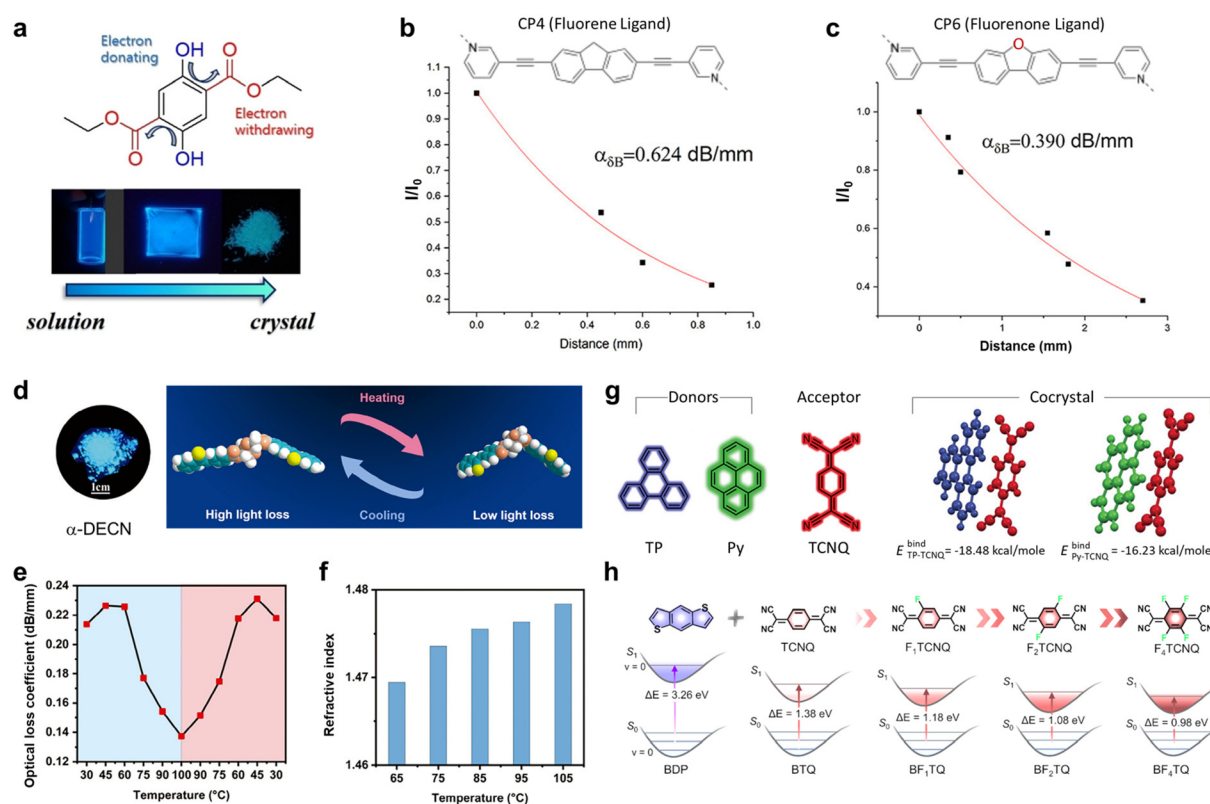


**FIG. 4.** Molecular design strategies for enhancing optical waveguiding properties. (a) Photoluminescence (PL) of diethyl 2,5-dihydroxyterephthalate was achieved through symmetric functionalization with electron-donating (EDG) and electron-withdrawing (EWG) groups. Top: molecular structure; bottom: photographic images of the diethyl 2,5-dihydroxyterephthalate in solution, film, and crystal powder forms under 365 nm UV illumination.<sup>81</sup> Reproduced with permission from Cho *et al.*, ChemPlusChem **84**, 1130 (2019). Copyright 2019 John Wiley and Sons. (b) and (c) Influence of ligand chemical composition on waveguiding in coordination polymers. Molecular structures and optical loss per distance of fluorene-derived pyridyl ligand (2,7-bis(pyridin-3-ylethynyl)-9H-fluorene) (b) and fluorenone-derived pyridyl ligand (2,7-bis(pyridin-3-ylethynyl)fluorene-9-one) (c). Reproduced with permission from Podda *et al.*, JACS Au **5**, 727 (2025). Copyright 2025 Author(s), licensed under a Creative Commons Attribution (CC BY) license. (d)–(f) Strategy for achieving high efficiency waveguiding at high temperature (100 °C) using self-assembled luminescent liquid crystals (LLC). (d) Photographic image captured under 365 nm UV lamp illumination paired with a schematic of the structural transition during the thermal cycle of an LLC composed of cyanostilbene and alkyl chains (a-DECN). (e) Variation of optical loss coefficient during heating and cooling processes, reflecting increased molecular mobility and a higher dipole moment as the opening angle decreases at elevated temperatures. (f) Temperature-dependent refractive index, attributed to enhanced electronic polarization induced by thermally driven changes in molecular geometry.<sup>87</sup> Reproduced with permission from Xia *et al.*, Adv. Funct. Mater. **34**, 2312478 (2024). Copyright 2024 John Wiley and Sons. (g) Molecular structures and binding energies for co-crystallization of donor, triphenylene (TP) and pyrene (Py), and acceptor molecules [7,7,8,8-tetracyanoquinodimethane (TCNQ)].<sup>90</sup> Reproduced with permission from Chen *et al.*, Adv. Opt. Mater. **12**, 2400726 (2024). Copyright 2024 John Wiley and Sons. (h) Band structure modulation via fluorine substitution on acceptor molecules in co-crystals. Structures of donor benzo[1,2-b:4,5-b']dithiophene (BDP) and fluorinated acceptors (F<sub>x</sub>-TCNQ), and corresponding band diagrams.<sup>67</sup> Reproduced with permission from Yu *et al.*, J. Am. Chem. Soc. **146**, 11845 (2024). Copyright 2024 American Chemical Society.

Molecular design also affects crystal packing and lattice spacing of the structure, which are key determinants of optical properties such as refractive index and birefringence.<sup>82</sup> Tighter crystal packing and reduced lattice spacing generally lead to higher refractive indices due to increased electronic polarizability, while anisotropic arrangements of molecules induce birefringence through direction-dependent refractive index variations.<sup>83</sup> These parameters are vital for optimizing TIR within the waveguide, thereby minimizing optical losses. While molecular packing and lattice spacing are widely recognized as key factors influencing optical properties, additional parameters also play roles in determining waveguiding efficiency. For instance, controlling crystallographic orientation and molecular packing modes in coordination polymers (CPs) significantly enhances their waveguiding efficiency. Rational modulation of coordination bonds and supramolecular  $\pi$ – $\pi$

interactions in fluorene-based CP crystals results in exceptionally low optical loss by preserving lattice integrity and controlling molecular orientation.<sup>63</sup> Notably, CPs containing fluorenone moieties exhibit lower attenuation coefficient relative to their fluorene-containing counterparts, and comparisons between polymorphs with identical chemical compositions reveal that chemical connectivity plays a more decisive role in waveguiding characteristics than do variations in molecular arrangement [Figs. 4(b) and 4(c)]. This phenomenon arises from variations in electronic coupling and transition dipole alignment, which are influenced by the distinct coordination environments. Although closely packed micro- or nanocrystalline structures can enhance surface morphology and crystallinity, excessive intermolecular coupling potentially results in exciton quenching and reduced radiative efficiency.



Molecular design strategies that induce large Stokes shifts have proven effective at mitigating reabsorption losses. CPs incorporating fluorenone ligands exhibit significantly lower optical losses compared to their fluorene-based counterparts, as the enlarged Stokes shift reduces the spectral overlap between absorption and emission bands.<sup>63</sup> This spectral decoupling suppresses self-absorption during photon propagation, thereby maintaining emission intensity and extending the effective waveguiding distance. Consistent with these observations, organic crystals with limited Stokes shifts show distance dependent redshifts that highlight the detrimental effect of spectral overlap on optical transmission.<sup>84</sup> Similarly, co-crystal systems with redshifted emission profiles demonstrate stable waveguiding behavior over extended distances, indicating the critical role of reduced reabsorption in maintaining optical fidelity.<sup>66</sup> These findings confirm the importance of designing molecular systems with asymmetric electronic transitions or strong CT characteristics to achieve large Stokes shifts and enhance waveguiding performance.

Another promising approach for developing active waveguides involves utilizing dynamic dipole moments by designing luminescent liquid crystals (LLCs) at the molecular level. Enhancing the dynamic dipole moment in LLCs substantially influences optical waveguiding by modulating molecular packing<sup>85</sup> and lattice spacing,<sup>86</sup> which in turn allows for precise control over the refractive index and a reduction in optical losses. For instance, temperature-induced variations in the dipole moment of LLCs can trigger reversible phase transitions between crystalline phases [Fig. 4(d)].<sup>87</sup> As shown in Figs. 4(e) and 4(f), these structural transitions optimize the refractive index profile, enhance TIR, and suppress scattering losses, thereby improving waveguiding performance, particularly at elevated temperatures. Consequently, exploiting the unique phase behavior and dynamic dipole characteristics of LLCs provides a robust strategy to engineer efficient optical waveguides for various optoelectronic applications.

While photophysical properties relevant to optical waveguiding can be tailored at the single-molecule level, introducing CT interactions through dopant incorporation provides practical advantages. This approach enhances structural integrity, promotes intermolecular electronic coupling, and enables long-range optical functionality without compromising host crystallinity.<sup>88,89</sup> CT cocrystal design that combines donor and acceptor molecules in a single crystalline film has enabled the organic heterostructures that exhibit near-infrared (NIR) emission with minimized waveguiding losses. This is achieved through finely tuned CT interactions and lattice matching between molecules [Fig. 4(g)].<sup>90</sup> For instance, CT cocrystals are formed by co-assembling electron donor molecules, triphenylene (TP), pyrene (Py), with the acceptor 7,7,8,8-tetracyanoquinodimethane (TCNQ). The relatively small differences in intermolecular binding energies, TP-TCNQ ( $E_{\text{bind}} = -18.48$  kcal/mole) and Py-TCNQ ( $E_{\text{bind}} = -16.23$  kcal/mole), allow these components to co-assemble while minimally disrobing the crystal integrity. Moreover, as dopant concentration increases, heterogeneous crystal growth occurs preferentially along a crystallographic plane with minimal lattice mismatch. This compatibility facilitates the formation of CT cocrystal with seamless interfaces, crucial for reducing scattering losses and preserving coherent photon propagation in waveguiding applications.

Furthermore, structural modification of the acceptor molecules within CT cocrystals offers an effective strategy for fine-tuning the electron density distribution across the  $\pi$ -conjugated framework.<sup>67</sup>

Such structural ordering substantially suppresses nonradiative recombination while enhancing the efficiency of radiative exciton recombination, and narrows the optical bandgap. For instance, in CT cocrystals composed of benzo[1,2-b:4,5-b']dithiophene (BDP, donor) and TCNQ (acceptor), stepwise fluorination of the TCNQ core induces a progressive redshift in the emission [Fig. 4(h)]. In addition to this spectral tuning, the increased number of fluorine atoms elevates the electron-withdrawing strength of the acceptor, thereby strengthening CT interactions with the donor. Moreover, face-to-face stacking promotes enhanced molecular alignment for charge transport, thereby optimizing optical waveguiding pathways within the crystal lattice. Collectively, meticulous structural control, combined with optimized intermolecular interactions, effectively minimizes exciton quenching and reabsorption losses, thereby enhancing photoluminescence (PL) quantum yields and extending propagation distances within waveguides. Thus, the molecular and structural optimization of organic heterostructures and CT cocrystals represents a robust approach for developing advanced, low-loss organic waveguides.

Despite substantial advances in molecular design for efficient waveguiding, intrinsic stability remains a critical challenge. Photooxidation generates defect states and parasitic absorption centers that progressively deteriorate optical performance. In addition, thermally induced lattice disorder disrupts intermolecular coupling and induces refractive-index fluctuations, while exciton-exciton annihilation accelerates nonradiative losses under high excitation densities.<sup>64,91-93</sup> These degradation pathways not only deteriorate emission quantum yields but also induce scattering centers that increase propagation losses during continuous operation. To mitigate these effects, several stability-oriented molecular design strategies have been demonstrated, such as perfluorination, halogen bonding, supramolecular locking, and rigidified core architectures.<sup>89,94,95</sup> These approaches enhance stability by lowering the susceptibility of  $\pi$ -conjugated backbones to oxidative attack, suppressing structural reorganization under heat, and preserving lattice integrity against morphological degradation. Such stability-oriented approaches highlight that the design principles enabling efficient light emission are not always sufficient to ensure long-term optical functionality. Consequently, continued efforts toward integrating stability considerations at the molecular design stage are indispensable for translating fundamental photophysical advances into practical waveguiding devices, underscoring the high value of reconciling efficiency with long-term robustness in organic photonic materials.

## B. Structural design

The structure of active organic waveguides can be broadly divided into two categories: single-component crystals and heterojunction-based structures. Single-component crystals provide rigidity through uniform crystallinity but remain susceptible to external damage, motivating strategies such as polymer encapsulation and slip-plane engineering for added flexibility.<sup>96</sup> In contrast, heterojunction-based active waveguides comprising two or more distinct substructures retain the intrinsic optical and electrical properties of their individual constituents, such as luminescence wavelength, energy transfer, and donor/acceptor characteristics, while simultaneously generating synergistic interactions. This multi-component configuration not only maintains the individual merits of each constituent but also enables overall

functionality, potentially facilitating novel applications in bio-imaging, sensing, multicolor emission, logic gating, and others.<sup>66,97,98</sup>

Achieving high-performance heterojunction active waveguides requires careful selection of molecules with similar physical and chemical properties, such as size, shape, and intermolecular interactions, to ensure compatibility along the channel and mitigate aggregation-caused quenching (ACQ),<sup>99</sup> an unintended luminescence suppression. In parallel, optimization of nucleation mechanisms and growth conditions is crucial to achieve uniform crystallization, thereby preventing phase separation and the formation of structural defects.<sup>100</sup> Energy band alignment of the constituent molecules must also be meticulously engineered to avoid mutual luminescence quenching, which can otherwise compromise both the light transmission efficiency and signal integrity.<sup>101–103</sup>

Ensuring structural stability in heterogeneously integrated materials requires effective molecular arrangement among the constituent phases. Notably, each constituent crystal within a heterogeneous system can independently exhibit either H- or J-type molecular aggregation, depending on its intrinsic packing geometry and a balance of non-covalent interactions, including van der Waals forces, electrostatic and dipole-dipole interactions, and halogen bonding. In H-aggregation, molecules adopt a parallel, face-to-face arrangement, whereas J-aggregation is characterized by head-to-tail stacking. These aggregation modes are often distinguished by the angle between the

transition dipole moment and the aggregation axis: angles exceeding  $54.7^\circ$  generally favor H-aggregation, while angles below promote J-aggregation. The distinctive photophysical behavior arises from the fact that in H-aggregates, the lower energy state induced by Davydov splitting is forbidden due to out-of-phase transition dipole moment oscillation, causing a blue shift of the absorption spectra, whereas J-aggregates possess allowed lower excited states that produce a red shift in the absorption spectra.<sup>104</sup> Thus, such heterojunction-based systems hold significant promise for diverse applications of photonic signal coupling.<sup>105,106</sup>

Figure 5(a) shows a sequential self-assembly approach that preserves the intrinsic properties of each constituent while constructing multi-component systems with the targeted structure and composition.<sup>11</sup> This method involves the stepwise integration of distinct organic molecules to achieve both homogeneous nucleation and precise control over non-covalent interactions.<sup>107,108</sup> For instance, under specific lattice matching conditions and balanced surface-interface energies, triblock nanowires (TNWs) are formed by longitudinal epitaxial growth at lower temperatures, whereas core/shell nanowires emerge via horizontal epitaxial growth at relatively higher temperatures. In this context, green-emissive nanowires composed of 4,4'-((1E,1'E)-(2,5-dimethoxy-1,4-phenylene)bis(ethene-2,1-diyl))dipyridine (DPEpe) and 1,4-diiodotetrafluorobenzene (F4DIB), as well as red-emissive nanowires assembled from DPEpe and 4-bromo-

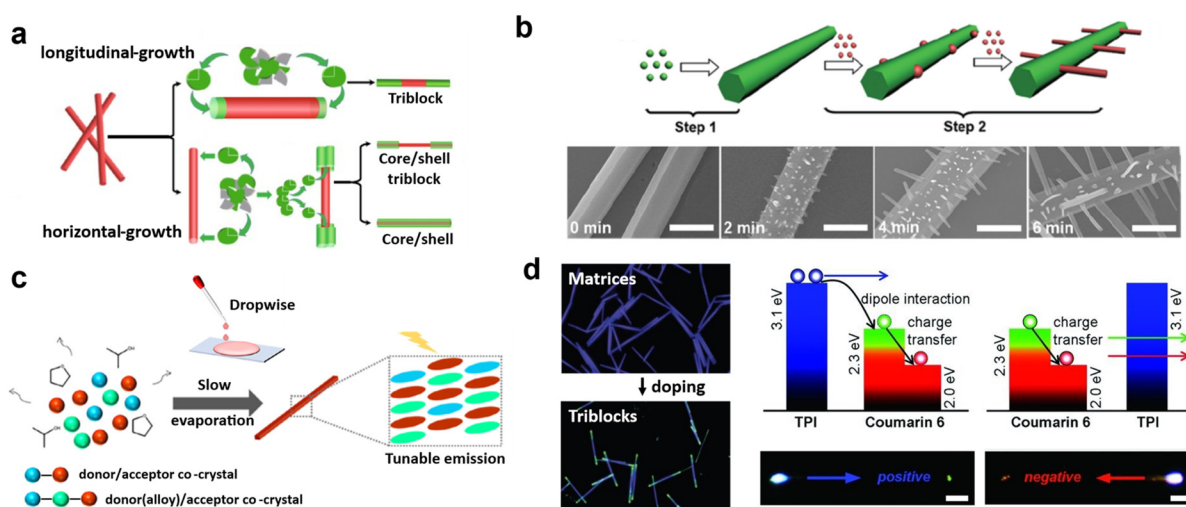


**FIG. 5.** Demonstration of multi-component structures for active waveguides. (a) Material integration enables the fabrication of triblock structures via longitudinal growth, whereas horizontal growth permits the formation of either a core/shell triblock or a fully developed core/shell crystal.<sup>11</sup> Green-emissive nanowires composed of 4,4'-((1E,1'E)-(2,5-dimethoxy-1,4-phenylene)bis(ethene-2,1-diyl))dipyridine (DPEpe) and 1,4-diiodotetrafluorobenzene (F4DIB), as well as red-emissive nanowires assembled from DPEpe and 4-bromo-2,3,5,6-tetrafluorobenzoic acid (BrFTA), are formed via halogen-bonding-driven self-assembly and serve as the structural components for these heterostructures. Reproduced with permission from Zhuo *et al.*, Nat. Commun. **10**, 3839 (2019). Copyright 2019 Author(s), licensed under a Creative Commons Attribution (CC BY) license. (b) In a two-step process, a backbone structure composed of aluminum tris(8-hydroxyquinoline) (Alq<sub>3</sub>) is first established, followed by the perpendicular outgrowth of 1,5-diaminoanthraquinone (DAAQ) branches on its surface, forming a dendritic co-crystal. All scale bars are 2  $\mu\text{m}$ .<sup>7</sup> Reproduced with permission from Zheng *et al.*, J. Am. Chem. Soc. **134**, 2880 (2012). Copyright 2012 American Chemical Society. (c) Mixed solution of red (acceptor), green, and blue (donor) materials is dropped onto a substrate, and slow evaporation enables compositional tuning to yield a full-color tunable crystal.<sup>110</sup> The donors include pyrene (Py) and fluoranthene (Flu), while the acceptors consist of tetracyanoquinodimethane (TCNB), tetrafluoroterephthalonitrile (TFP), and octafluoronaphthalene (OFN). Reproduced with permission from Qi *et al.*, Aggregate **5**, e411 (2024). Copyright 2024 Author(s), licensed under a Creative Commons Attribution (CC BY) license. (d) One-dimensional crystals based on 2,4,5-triphenylimidazole (TPI) with tunable emission colors were fabricated by adjusting the doping ratio of the dopant 3-(2-benzothiazolyl)-7-diethylaminocoumarin (coumarin 6). The right panel illustrates exciton conversion from TPI to coumarin 6. Under 351 nm laser excitation at the lightly doped left end (positive case) and the heavily doped right end (negative case), high-energy photons (blue emission) propagate only in the positive direction due to the energy gap difference. (Scale bar: 5  $\mu\text{m}$ ).<sup>111</sup> Reproduced with permission from Zhang *et al.*, Adv. Mater. **25**, 2854 (2013). Copyright 2013 John Wiley and Sons.

2,3,5,6-tetrafluorobenzoic acid (BrFTA), are formed via halogen-bonding-driven self-assembly. These two distinct nanowires serve as the building blocks for TNWs and C/S-NWs. Furthermore, by precisely modulating the formation ratio of hydrogen and halogen bonds, it is possible to quantitatively control the length of the red-emissive segment in TNWs and the degree of core exposure at the center of C/S-NWs. In a related sequential strategy, the two-step growth process shown in Fig. 5(b), also a form of sequential assembly, has been used to produce dendritic organic heterojunctions by incorporating distinct backbone and branch components, such as aluminum tris(8-hydroxyquinoline) ( $\text{Alq}_3$ ) as the backbone and 1,5-diaminoanthraquinone (DAAQ) as the branch.<sup>7,109</sup> These results highlight the versatility of controlled sequential processes in engineering complex heterostructures.

Molecular co-crystal alloys (MCAs) leverage the compositional tunability of organic alloys with unique optical properties, such as anisotropic polarization and high quantum yield. As illustrated in Fig. 5(c), MCAs represent a multi-component crystal system based on binary electron donor/acceptor pairs, such as Py and fluoranthene (Flu) as donors, and tetracyanoquinodimethane (TCNB), tetrafluoroterephthalonitrile (TFP), and octafluoronaphthalene (OFN) as acceptors.<sup>110</sup> The continuous and orderly molecular stacking enabled by a mixed-solvent evaporation technique promotes efficient charge transport. Furthermore, by tuning the molar ratio of the donor component, continuous fluorescence emission covering the red, green, and blue regions can be achieved. However, the synthesis of MCAs requires consideration of molecular size compatibility and similar binding energies between each molecule to preserve crystallinity and prevent phase separation for achieving full-color luminescence in organic active waveguides with low optical loss coefficients.

Figure 5(d) illustrates an alternative approach, liquid-phase co-assembly, for fabricating color-gradient organic microtubes with axially controlled doping concentrations of donor and acceptor.<sup>111</sup> In the absence of dopants, the aggregates of TPI exhibit a one-dimensional (1D) morphology with uniform blue emission [left panel of Fig. 5(d)]. However, the introduction of a minor fraction (0.5 mol. %) of the acceptor 3-(2-benzothiazolyl)-7-diethylaminocoumarin (coumarin 6) results in selective doping at both ends of the tube, leading to green-blue-green triblock structures [middle panel of Fig. 5(d)]. Furthermore, by modulating the diffusion of acceptor molecules and controlling the co-assembly kinetic via sonication, it diversifies the longitudinal color distribution within the microtubes. Upon laser excitation in the donor region, excited-state energy is efficiently transferred to the acceptor through dipole-dipole interactions, generating acceptor excitons that subsequently recombine radiatively to emit green photons. In contrast, direct excitation of acceptor, which features a relatively narrow energy gap, precludes reverse energy transfer to the donor due to the unfavorable energetic alignment [right panel of Fig. 5(d)]. This unidirectional exciton migration gives rise to a diode-like photonic response, where the presence or absence of energy transfer, depending on the excitation location, enables on/off behavior analogous to an electronic diode. However, the fabrication of such optical heterostructures remains challenging due to morphological and crystallographic mismatches that potentially induce structural defects and substantial optical losses. Therefore, the implementation of precise self-assembly strategies and controlled crystal growth techniques is essential for the optimization of these structures.

In summary, the structural design of heterojunction-based active waveguides plays a critical role in determining their optical performance, as molecular arrangement, crystallinity, and phase compatibility directly govern light propagation, confinement, and emission. Precise control over non-covalent interactions, such as  $\pi$ - $\pi$  stacking, hydrogen/halogen bonding, and van der Waals forces, enables the formation of ordered multi-component organic crystals with minimal defects and optimal energy band alignment. Such structural control is essential not only for maintaining the individual optical functions of each component but also for unlocking emergent properties via synergistic coupling for active waveguides, such as directional light propagation, which can be harnessed to construct optical logic gates or route energy and signal flow to designated locations for interconnection with other components.

### C. Fabrication and integration

The practical use of active organic waveguides in optoelectronic systems depends not only on molecular and structural design but also on their ability to be integrated with external components such as light sources, detectors, and microelectronic circuits. Fabrication strategies therefore must address three interrelated challenges: achieving deterministic alignment of waveguides, ensuring efficient optical and electrical coupling with surrounding devices, and developing integration processes that are compatible with standard microelectronics fabrication and packaging technologies.

A central requirement is the ability to align organic crystals along predetermined axes so that their guided modes can be efficiently coupled to external sources. Techniques such as confinement-assisted solution growth, surface-energy patterning, and epitaxial alignment have enabled deterministic orientation of nanowires and micro-ribbons along optical axes, thereby maximizing coupling efficiency with incident beams.<sup>112</sup> Template-assisted assembly and micromanipulation extend this control by placing individual crystals directly at pre-defined locations on a chip, a prerequisite for positioning them adjacent to emitters or detectors.<sup>113</sup> These advances are particularly important for butt-coupling organic waveguides to on-chip light sources such as edge-emitting organic lasers and inorganic semiconductor lasers, where misalignment would otherwise result in severe coupling losses.

Once alignment is established, the next challenge is coupling organic waveguides with detectors and other functional elements. Two routes have been explored. In one, electrodes are first patterned on the substrate, and organic crystals are subsequently transferred or laminated across the electrode gap. Nondestructive transfer printing using elastomeric stamps [such as polydimethylsiloxane (PDMS)] provides gentle relocation of crystals, while mechanical lamination achieves precise positioning with compatibility across a variety of electrode geometries.<sup>114</sup> In the other route, crystals are grown *in situ* on substrates such as  $\text{Si}/\text{SiO}_2$  or indium phosphide (InP), followed by electrode deposition.<sup>115,116</sup> This approach enables direct interfacing of waveguides with photodiodes or transistor circuits fabricated in the same process line. Refinements such as selective transfer of pre-patterned gold films or deposition along specific crystal facets allow the formation of directional couplers, polarization-sensitive junctions, and contact geometries that minimize scattering losses while ensuring efficient charge extraction. In this way, optical signals guided within organic crystals can be converted directly into electrical signals in



adjacent photodetectors or routed to light-emitting devices for re-emission.

Beyond sequential growth and integration, recent work has focused on strategies that unify crystal assembly with device fabrication to further simplify the fabrication process. For example, sequential solution self-assembly combined with selective etching has been used to create chip-scale heterostructures composed of one- and two-dimensional organic crystals that support multidirectional optical routing and multi-terminal outputs.<sup>117</sup> These monolithic processes reduce alignment tolerances and open a pathway to integrating organic waveguides with multi-port detectors or multiplexed light sources. Similarly, template-guided physical vapor transport on substrates patterned with silicon nanogrooves or pillar arrays directs crystal growth into predefined channels, yielding mechanically robust and optically aligned structures that can interface directly with detectors positioned at the channel ends.<sup>118–121</sup> Such approaches mimic the lithographic precision of conventional photonics, thereby offering compatibility with microelectronic packaging.

A critical question is whether organic waveguides can be incorporated into established semiconductor manufacturing environments such as CMOS platforms. While organic semiconductors lack the robustness of silicon, advances in template-free integration methods, such as inkjet printing with micrometer-level placement accuracy and two-photon polymerization lithography with sub-micrometer resolution, are beginning to close this gap.<sup>39,122–124</sup> These techniques allow organic crystals or hybrid organic–inorganic waveguides to be patterned directly on CMOS-compatible substrates without post-alignment steps, facilitating direct coupling to silicon photodetectors, light modulators, and microelectronic interconnects. Moreover, flexible transfer-printing processes are compatible with back-end-of-line (BEOL) packaging, offering opportunities for embedding organic waveguides into heterogeneous integration schemes alongside silicon photonics.<sup>125,126</sup>

In summary, fabrication and integration strategies for organic active waveguides are evolving from simple crystal growth toward fully integrated device platforms that couple efficiently to external light sources and detectors while remaining compatible with microelectronics fabrication. Deterministic alignment ensures low-loss coupling, electrode integration enables direct optical-to-electrical interfacing, and template-guided or printing-based assembly provides pathways to CMOS compatibility. These advances collectively suggest that organic waveguides, though delicate at the molecular level, can be positioned as functional building blocks within high-speed, low-power photonic integrated circuits—provided that alignment, coupling, and long-term stability challenges can be fully addressed.

#### IV. APPLICATION OF ACTIVE WAVEGUIDE USING ORGANIC SEMICONDUCTORS

##### A. Optical sensors

Recent advances in organic semiconductor-based optical sensors have emphasized the utility of dynamically modulating light within organic microstructures, thereby offering enhanced functionality for sophisticated sensing applications. Organic materials, by virtue of their flexibility,<sup>84</sup> sensitivity to environment,<sup>127,128</sup> and molecular design versatility,<sup>129</sup> exhibit measurable responses to a broad range of stimuli, including thermal fluctuations, mechanical deformations, and biomolecular interactions, which permits real-time, remote, and highly

selective detection. Such characteristics render organic waveguide-based sensors invaluable for applications spanning molecular diagnostics to environmental monitoring.

Recent work has demonstrated that DNA recognition can be sensitively probed through waveguiding properties of 1D hybrid organic microcrystals.<sup>8,130</sup> Specifically, single-strand DNAs (ssDNAs) are incorporated onto the crystal surface during the self-assembly of Alq<sub>3</sub> into prismatic hexagonal rods, making the waveguide bioresponsive. Upon hybridization with perfectly matched target DNAs (tDNAs), the PL intensity of the Alq<sub>3</sub> microcrystal increases by fivefold.<sup>131</sup> This enhancement is attributed to the formation of an approximately 120-nm thick double-strand DNA crust that suppresses non-radiative decay by reducing exciton quenching and improving light confinement. As a result, a reduction in the optical loss coefficient was observed, from 0.244 to 0.159  $\mu\text{m}^{-1}$ , confirming an improved waveguiding. To evaluate how waveguiding behavior responds to sequence-specific hybridization, comparative experiments were performed using perfectly matched and 1-mer mismatched tDNAs. Complementary atomic force microscopy (AFM) cantilever experiments, in which different types of DNA were selectively attached to the opposing ends of a single Alq<sub>3</sub> microcrystal, further confirmed the robust remote DNA sensing capabilities of the active organic waveguide, with discernible differences in PL intensities observed along the opposing ends of a single waveguide when exposed to mismatched vs perfectly matched DNA [Fig. 6(a)].

In a separate study, a remote biosensing system was demonstrated through the hybridization of 1,4-bis(3,5-bis(trifluoromethyl)styryl)-2,5-dibromobenzene (TSDB) with CdSe/ZnS quantum dots (QDs).<sup>24</sup> The system functioned as a photonic biosensor by guiding the distinct emission responses from sulfo-cyanine3 (Cy3)-labeled oligonucleotides anchored at the distal end of the waveguide. This guided emission was remotely triggered by the presence or absence of QDs at the excitation site, highlighting the waveguide's capacity for spatially resolved signal transduction. In this configuration, TSDB functions as the waveguide medium, facilitating the transmission of luminescence despite the unfavorable electronic band alignment between the two materials (QDs: HOMO of 6.0 eV, LUMO of 4.0 eV; TSDB: HOMO of 5.89 eV, LUMO of 2.90 eV). When the TSDB/green-emitting QD hybrid interface was excited with a 405 nm laser, the PL emissions propagated along the TSDB, and an additional emission peak at 532 nm was observed at the detection region. The QD emission transmitted through the TSDB waveguide subsequently induced FRET to Cy3 molecules ( $\lambda_{\text{abs}} = 554 \text{ nm}$ ) anchored at the distal end, which exhibited strong fluorescence with a maximum at 580 nm. Furthermore, efficient coupling between QD and TSDB nanowires was confirmed by a nearly threefold increase in PL intensity at 580 nm, compared to the case without QDs, along with a shoulder peak at 532 nm attributed to enhanced absorption by the Cy3 fluorescence dye [Figs. 6(b) and 6(c)]. These results highlight the potential of actively tunable photonic systems that go beyond conventional organic semiconductor waveguides, as evidenced by efficient long-range energy relay from QDs to Cy3 fluorophores through guided PL.

In addition to intrinsic modulation of guided PL, active sensor functionality has been achieved via morphology-dependent shifts in emission wavelength. For example, a structurally integrated system of elastic light-emitting organic crystals and a mechanically responsive polymer allows dynamic control over the outcoupling position of the



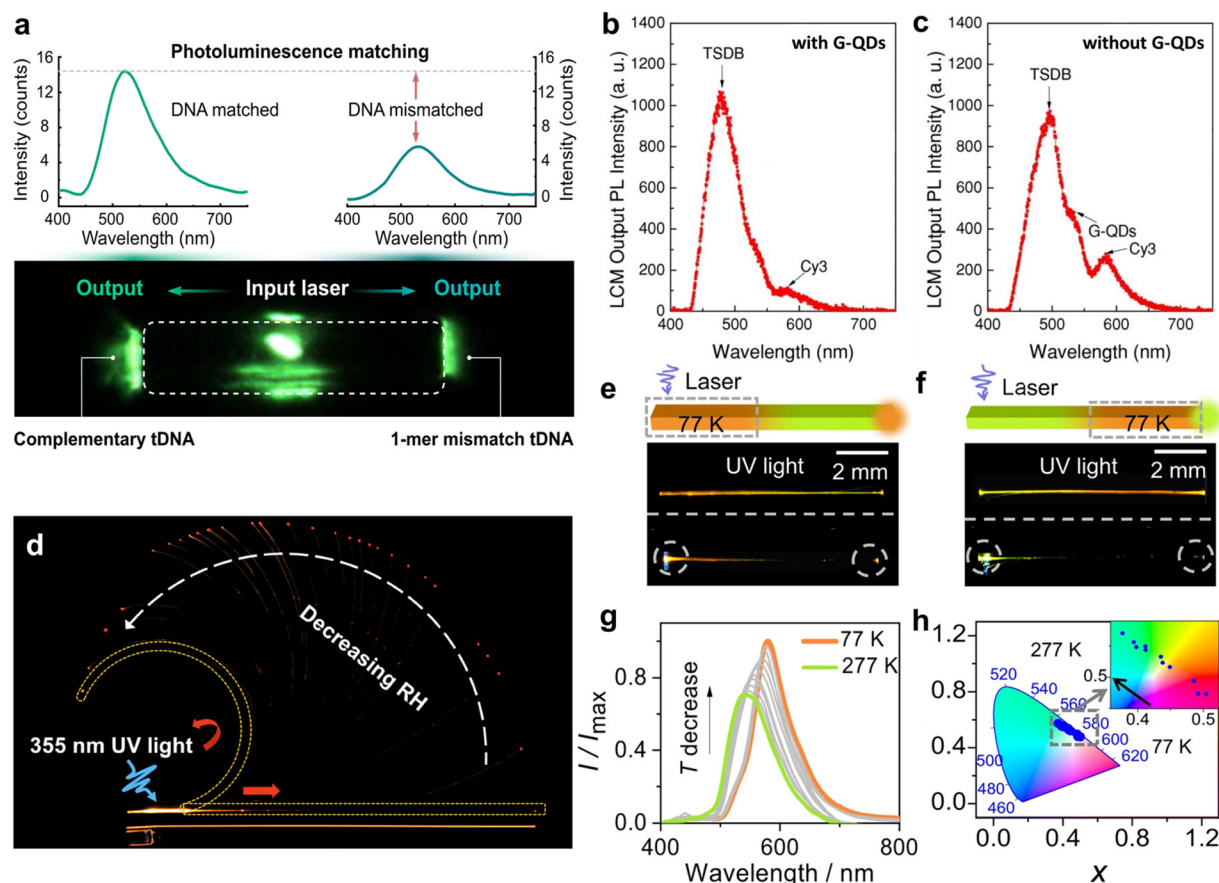


**FIG. 6.** (a) Photoluminescence (PL) spectrum and color image of 1D tris(8-hydroxyquinoline)aluminum(III) ( $\text{Alq}_3$ ) hexagon crystal interface with perfectly matched target DNA (tDNA) and 1mer mismatched tDNA.<sup>8</sup> Reproduced with permission from Kim *et al.*, *Adv. Mater.* **20**, 2070334 (2020). Copyright 2020 John Wiley and Sons. (b) and (c) PL spectra of 1,4-bis(3,5-bis(trifluoromethyl)styryl)-2,5-dibromobenzene (TSDB) nanowire (NWs) (b) and TSDB/green emitting quantum dots (G-QD) hybrid NW (c) for remote biosensing; in the hybrid configuration, the localized G-QDs at the excitation site enhance Cy3 emission via energy transfer.<sup>24</sup> Reproduced with permission from Cho *et al.*, *Adv. Funct. Mater.* **24**, 3684 (2014). Copyright 2014 John Wiley and Sons. (d) Polymer-coated elastic organic waveguide fixed at one end, where light output is modulated by humidity driven bending. Initially bent under low humidity, the crystal gradually straightens as relative humidity (RH) increases at 20 °C under 355 nm laser excitation. Yellow dashed lines and red arrows indicate crystal contours and the corresponding light paths before and after straightening.<sup>132</sup> Reproduced with permission from Lan *et al.*, *Angew. Chem. Int. Ed.* **61**, e202200196 (2022). Copyright 2022 John Wiley and Sons. (e) and (f) Schematic and photographic images of indole-chalcone-derived crystal during optical waveguide experiment with excitation at 77 K (e) and detection at room temperature, and excitation at RT and detection at 77 K (f). (g) Emission spectra of indole-chalcone-derived crystal measured at various temperatures. (h) CIE 1931 color space coordinates plotting the emission of the crystal at different temperatures. *Inset*: Zoomed view of the highlighted region.<sup>133</sup> Reproduced with permission from Di *et al.*, *Nat. Commun.* **13**, 5280 (2022). Copyright 2022 Author(s), licensed under a Creative Commons Attribution (CC BY) license.

waveguided emission in response to external stimuli. Building on this concept, recent studies have demonstrated 1D humidity-responsive structures that integrate organic crystals, moisture-responsive polymers, and cladding polymer layers, fabricated as composite waveguides.<sup>132</sup> The fluorescent organic crystals serve as the waveguiding core, possessing elastic moieties formed by hydrogen bonding between OH and CH=N groups, which promote a planar conjugated skeleton favorable for  $\pi$ -stacking. These structures are further modified by sequential coating with poly(diallyldimethylammonium) (PDDA) and poly(styrenesulfonate) (PSS), which function as ionic cladding layers to stabilize the architecture and confine the guided modes. Subsequent encapsulation with a polyvinyl alcohol (PVA) layer imparts humidity responsiveness, enabling the waveguiding path to

reversibly transition from linear to curved configurations under varying relative humidity (RH) conditions [Fig. 6(d)]. Quantitative analysis of curvature extracted from optical imaging exhibited excellent linearity with detection limits in the RH range of 0.129 to 0.166%. When excited with a 355 nm pulsed laser, these crystals exhibited a spectral shift from orange to red primarily due to partial reabsorption, while maintaining stable optical waveguiding properties with optical loss coefficients of approximately 0.43 to 0.44 dB/mm<sup>-1</sup> under varying humidity conditions. Parallel experiments confirm the capability of these hybrid materials to function as active optical waveguides with humidity-tunable light directionality.

Furthermore, a fluorescence-based thermal sensing system using elastic organic crystals has been demonstrated.<sup>133</sup> Constructed from

$\pi$ -conjugated molecules, these mechanically flexible crystals, (E)-1-(3,5-bis(trifluoromethyl)phenyl)-3-(1-ethyl-1H-indol-3-yl)prop-2-en-1-one, operate across a range of 77 to 277 K, making them viable for extreme environments such as space exploration. In addition, these elastic organic crystals exhibited intrinsic optical waveguiding behavior that was independent of the temperature at the detection point, with the emission wavelength solely determined by the temperature at the excitation site. This decoupling of excitation and detection enables directional signal transduction, which forms the basis for their thermal sensing functionality. Temperature sensing was achieved through a linear modulation of emission wavelength in response to temperature gradients. As illustrated in the top panels of Figs. 6(e) and 6(f), one end of a crystal was laser-excited while the same or the opposite end was cooled with liquid nitrogen to evaluate waveguiding performance. Under uniform UV illumination, distinct orange (580 nm) and green (550 nm) emissions were observed corresponding to the cold and warm regions, respectively [the middle panels of Figs. 6(e) and 6(f)]. Subsequent laser-induced propagation of these emissions across the crystal confirmed that the optical signal is determined by the local temperature [the bottom panels of Figs. 6(e) and 6(f)], while the emission blue shifted with decreasing intensity upon warming after cooling [Figs. 6(g) and 6(h)]. Even after 1000 bending cycles, the crystal maintained its sensitivity and structural integrity with a consistent optical loss coefficient under both mechanical bending and low-temperature conditions. These findings show the potential of organic crystals-based active waveguide as reliable alternatives to conventional and brittle temperature sensors.

## B. Lasing

For light amplification by stimulated emission through optical pumping, inorganic and organic microcavity resonators operate via fundamentally disparate mechanisms. Inorganic semiconductor microcavities, light amplification is achieved by stimulated emission within an active gain medium, while the surrounding cavity structure provides passive optical confinement to enhance feedback and reduce losses. In contrast, organic semiconductor microcavities serve as active gain media themselves as both the absorber of pump light and emitter, integrating gain and confinement within the same molecular framework.<sup>134,135</sup>

Lasing requires optical feedback and mode selection within the microcavity, achieved via controlled cavity geometry that comprises highly ordered self-assembled organic compounds. Organic compounds are self-assembled into ordered nanostructures including nanowires,<sup>136,137</sup> nanodisks,<sup>138</sup> and microspheres<sup>139,140</sup> through intermolecular interactions. The self-assembly of organics enables achieving preferential molecular alignment, which affects the efficient gain profile of active medium that leads to low-threshold room temperature lasing. Also, the flexible properties of organics enable mechanically flexible microcavities with tunable optical properties.

Recent demonstration of organic nanowire lasers includes the fabrication of single crystalline nanowire using TPI via physical vapor deposition (PVD), achieving smooth, defect-free morphology and robust active waveguiding [Fig. 7(a)].<sup>141</sup> These TPI nanowires exhibited significantly reduced full width half maximum (FWHM) of the PL spectra at room temperature, a phenomenon typically observed under cryogenic conditions. Stimulated emissions with well-defined cavity modes were observed beyond a threshold excitation density, confirming the transition from amplified spontaneous emission (ASE) to

multimode lasing [Fig. 7(b)]. The definition of these modes is strongly dependent on nanowire dimensions with thicker and longer wires producing more distinct resonances, thereby positioning TPI nanowires as promising candidates for nanoscale photonic devices.

Crystals that provide both mechanical elasticity and high fluorescence quantum yield have been developed by incorporating a guest fluorescent molecule (3,6-bis(octylamino)terephthalate) into a non-fluorescent host (2,5-dihydro-3,6-bis(octylamino)terephthalate).<sup>10</sup> The self-doped crystals, comprising a mechanically flexible host and a fluorescent guest that remains in the lattice due to structural similarity, are obtained from crude products in which the guest molecule forms as a minor oxidized by-product ( $\sim 3\%$ ) during synthesis and cannot be removed by recrystallization. These self-doped crystals, formed via solvent evaporation, maintain efficient optical waveguiding efficacy in both straight and bent states with minimal loss, and exhibit ASE under high excitation energy. The self-doped crystal shows a significant narrowing of its emission spectrum, from a FWHM of approximately 63 nm at low pump energy ( $150 \text{ kW cm}^{-2}$ ) to 10 nm at higher energy ( $650 \text{ kW cm}^{-2}$ ) [Fig. 7(c)], with ASE thresholds of  $150 \text{ kW cm}^{-2}$ , a performance retained in bent configuration [Fig. 7(d)], with a threshold of  $115 \text{ kW cm}^{-2}$ . Such robust ASE behavior under various shapes reinforces their potential for mechanically flexible active waveguide application.

A dual-color single-mode lasing system has been realized using axially coupled two heterogeneous organic nanowire resonators. In this configuration, two self-assembled single-crystal nanowires—cyano-substituted oligo(p-phenylenevinylene) (OPV-A) and cyano-substituted oligo( $\alpha$ -phenylenevinylene)-1,4-bis(R-cyano-4-diphenylaminostyryl)-2,5-diphenylbenzene (OPV-B)—each supporting multimode lasing when isolated, function as both gain media and spectral filters for one another when axially coupled [Fig. 7(e)].<sup>55</sup> By precisely tuning parameters such as nanowire length and the interwire spacing, effective optical coupling is achieved, leading to the selective amplification of desired modes. This approach enables high spectral purity and low-threshold lasing at both blue ( $\sim 458 \text{ nm}$ ) and green ( $\sim 555 \text{ nm}$ ) wavelengths [Figs. 7(f) and 7(g)]. In the coupled system, each nanowire produces single-mode emissions modulated by its partner while the intercavity gap functions as a shared outcoupling port for dual-color emissions [Fig. 7(h)]. This mutual mode selection not only eliminates multimode interference but also enables efficient photon delivery in miniaturized photonic circuits, thereby enhancing device integration.

## C. Optical signal manipulation

Optical logic operations are gaining attention as they enable faster and more efficient alternatives to conventional binary computing. Unlike traditional systems limited to binary logic states, optical logic gates offer multiple output states collected by illuminating spatially separated regions with a pump laser, each emission wavelength corresponding to a unique logic state, thereby increasing the information density. This functionality can be effectively realized using organic active waveguides, which offer fast propagation speed, minimal energy dissipation, reduced thermal generation, ultrafast nonlinear response, and compatibility with miniaturized on-chip systems.<sup>5,11,97,110,142–149</sup> Especially, wavelength shifts achieved through active organic waveguides enable efficient optical signal conversion by generating multiple output wavelengths from a single input, making them suitable for optical logic gate implementations. This wavelength shift is often realized

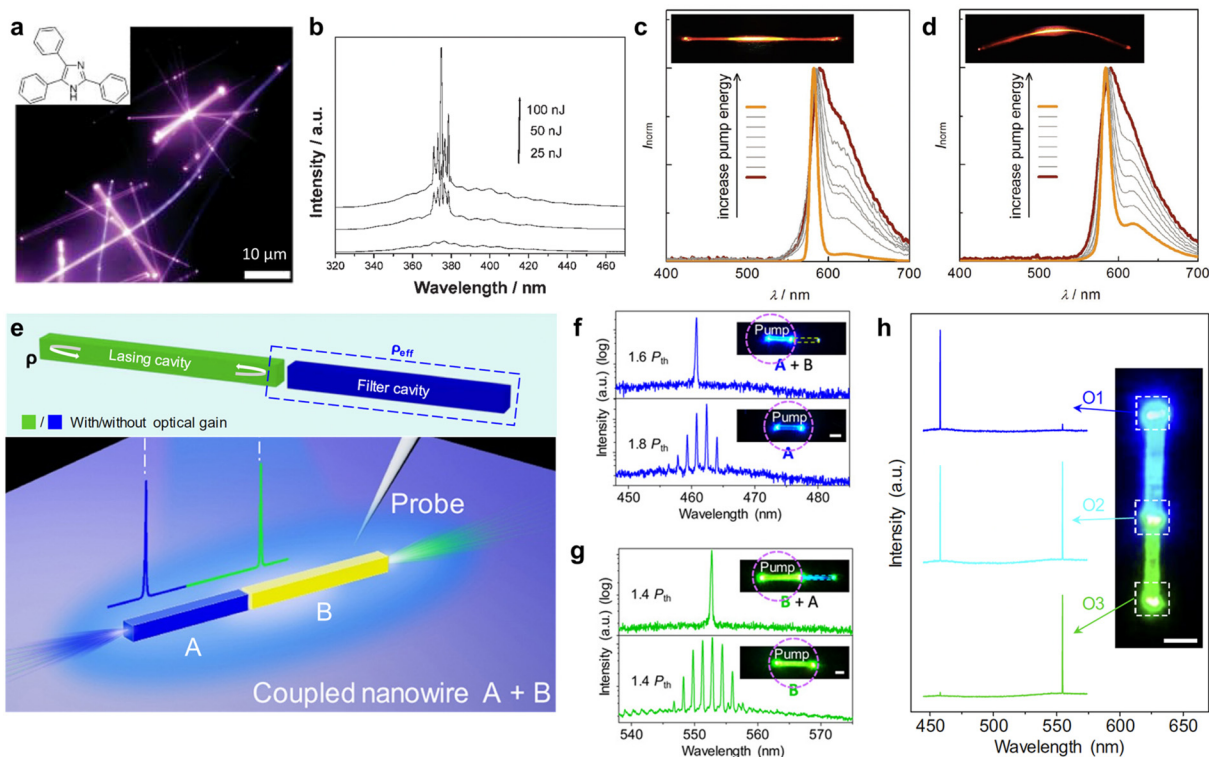


**FIG. 7.** (a) Molecular structure and PL image of 2,4,5-triphenylimidazole (TPI) nanowires (NWs). (b) Power dependent PL emission spectra of TPI NW (800 nm wide and 15  $\mu\text{m}$  long).<sup>141</sup> Reproduced with permission from Zhao *et al.*, *Adv. Mater.* **20**, 1661 (2008). Copyright 2008 John Wiley and Sons. (c) and (d) Powder dependent PL emission spectra and image of elastic self-doping organic single crystals composed of a guest (3,6-bis(octylamino)terephthalate) doped into a host matrix (2,5-dihydro-3,6-bis(octylamino)terephthalate) in their straight (c) and bent (d) states.<sup>70</sup> Reproduced with permission from Huang *et al.*, *Adv. Mater.* **30**, 1800814 (2018). Copyright 2018 John Wiley and Sons. (e) Schematic illustration of dual-color single-mode lasing in axially coupled organic NW resonators. (f) and (g) Lasing spectra of cyano-substituted oligo(p-phenylenevinylene) (OPV-A) (f) and cyano-substituted oligo(x-phenylenevinylene)-1,4-bis(R-cyano-4-diphenylaminostyryl)-2,5-diphenylbenzene (OPV-B) (g) NWs, showing a transition from multimode in non-coupled structure to single mode lasing when coupled. Insets: Corresponding PL images of individual OPV-A and OPV-B NWs and the coupled nanowire pairs under 400 nm laser excitation (scale bars, 5  $\mu\text{m}$ ). (h) PL spectra collected from three discrete outcoupling ports positioned at the intercavity gap (O2) and end facets of OPV-A (O1) and OPV-B (O3) (scale bar, 5  $\mu\text{m}$ ).<sup>55</sup> Reproduced with permission from Zhang *et al.*, *Sci. Adv.* **3**, e1700225 (2017). Copyright 2017 Author(s), licensed under a Creative Commons Attribution (CC BY) license.

in organic active waveguides through integrated multicomponent heterojunctions comprising different organic materials. Thus, integrating active waveguides within multicomponent heterojunctions allows spatial variations in excitation position along heterostructure nanowires to produce distinct output signals, thereby enabling sophisticated optical logic operations.<sup>11,97,145</sup>

High performance optical logic gates necessitate seamless integration of active waveguides, which require epitaxial growth of each system. However, it is challenging to achieve ordered epitaxial growth and controllable co-assembly within multicomponent systems, primarily due to lattice mismatches and weak non-covalent interactions. Recent advances have mitigated these issues by altering the substituents of acceptor molecules, listed in Fig. 8(a), thereby attaining excellent lattice matching.<sup>97</sup> Pairing a single donor molecule with a series of acceptor molecules bearing different substituents under slow crystalline growth process has enabled fine control over lattice matching, particularly by minimizing lattice matches between molecular components with diverse emission spectra, luminescence efficiencies, and fluorescence lifetimes. Under accelerated crystal growth

conditions, excess molecules tend to assemble on low-mismatch crystal facets. This facet-selective growth branch formation on the side surfaces of microwires enhances structural asymmetry and enables the generation of more complex optical codes. Materials other than organics have also been integrated into optical logic gate configurations such as microwires comprising QDs of green-emitting shell and red-emitting core. As shown in Fig. 8(b), when a 375 nm laser is directed at different positions on the branched core/shell microwire (inputs I and II), the resultant variation in the relative intensities of four outputs [Fig. 8(c)] can be encoded as distinct information channels [Fig. 8(d)].

The asymmetric transport of photons is crucial for the advancement of optical logic gates as it facilitates the generation of precise and complex optical signals by allowing unidirectional or preferential flow of light. Such asymmetry ensures that signal flow aligns with the intended logic pathways, allowing for selective activation of output channels. This directional control enhances signal fidelity and supports complex output configurations essential for advanced optical logic operations. As a result, extensive research has focused on branch formation as a means to enhance asymmetry.<sup>97,142,148</sup> Conventional 1D



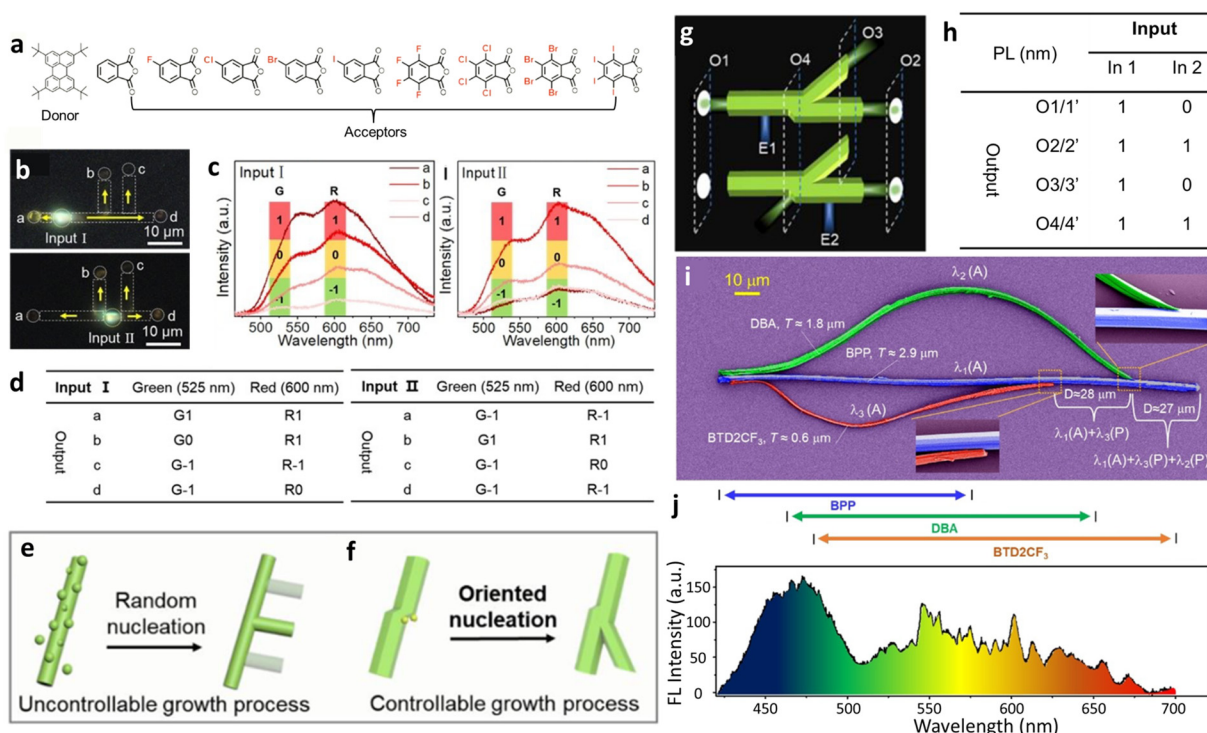


**FIG. 8.** (a) Molecular structures of donor and acceptor compounds with varied substituents. Lattice matching was achieved by altering the acceptor substituents without inducing significant structural deformation. Accordingly, the emission spectra are adjustable through combining donors with different acceptors. (b) PL image of the resultant cocystal under a 375 nm laser excitation. (c) Relative PL intensities at four distinct outputs depending on two different inputs. (d) Corresponding truth table for the optical logic gate implemented by cocystal.<sup>37</sup> Reproduced with permission from Lin *et al.*, *Angew. Chem. Int. Ed.* **62**, e202214214 (2023). Copyright 2023 John Wiley and Sons. (e) and (f) Contrast the uncontrolled random branch growth (e) with a guided branch growth strategy designed to enforce precise spatial positioning (f). (g) Varied optical waveguide propagation depending on the excitation input position. (h) Truth table for the optical logic gate governed by branch-controlled structural asymmetry.<sup>148</sup> Reproduced with permission from Ma *et al.*, *J. Am. Chem. Soc.* **145**, 9285 (2023). Copyright 2023 American Chemical Society. (i) Mechanical integration of an organic wavelength division multiplexer (WDM). (j) Optical spectrum measured at the end of organic waveguide, confirming the multiplexed output.<sup>150</sup> Reproduced with permission from Kumar *et al.*, *Angew. Chem. Int. Ed.* **61**, e202212382 (2022). Copyright 2022 John Wiley and Sons.

microstructures usually suffer from stochastic branch positioning [Fig. 8(e)], thereby precluding consistent asymmetric light propagation. This limitation has been overcome by engineering branch growth-controlled microstructures using CT cocrystals composed of electron-rich perylene and electron-deficient 2,4,6-trimethylbenzene-1,3,5-tricarbonitrile (TBT).<sup>148</sup> Utilizing the active surfaces of twinned microrods, organic molecules are directed to form branches at predetermined sites along the trunk [Fig. 8(f)]. Under 375 nm-laser irradiation, these structures exhibit distinct asymmetrical optical waveguide characteristics, even when the propagation lengths are identical [Fig. 8(g)]. The resultant anisotropic behavior enables the construction of a truth table [Fig. 8(h)], affirming the potential of these structures for intricate photonic applications.

Meantime, optical interconnects also arise as an important application of optical waveguides since integrating wavelength division multiplexers (WDM) with optical logic gates further enhances the computation capacity by enabling simultaneous multi-channel signal processing. This is enabled by the non-interfering nature of distinct wavelength channels, allowing efficient signal multiplexing. An example is a wide-bandwidth organic WDM designed for visible light communication (VLC), which incorporates three distinct molecular

emitters, 2,6bis(pyrazolyl) pyridine units connected to a biphenyl molecule (BPP) core, 9,10bis(bromo)anthracene (DBA), and (Z)-2-(3,5bis(trifluoromethyl)phenyl)-3-(7-methoxybenzo[c][1,2,5]thiadiazol-4-yl) acrylonitrile (BTD2CF<sub>3</sub>) [Fig. 8(i)].<sup>150</sup> These were precisely positioned side-by-side using an AFM cantilever tip. When the left side of the WDM structure is pumped with a 405 nm laser, a multiplexed fluorescence signal emerges from the right side of the BPP crystal, comprising three emission wavelengths ( $\lambda_1 + \lambda_2 + \lambda_3$ ), corresponding respectively to the emissions of BPP, DBA, and BTD2CF<sub>3</sub>, where  $\lambda_1$ ,  $\lambda_2$ , and  $\lambda_3$  [Fig. 8(j)]. This design extends the bandwidth of the BPP crystal waveguides from its original 420–570 to 420–700 nm, while preserving the intrinsic optical modes. As a result, this system offers a robust and efficient platform for multichannel data transmission in the visible light spectrum.

## V. CONCLUSION AND PERSPECTIVES

Organic active waveguides are evolving from scientific curiosities into versatile building blocks for photonic systems, driven by advances in molecular design, exciton-mediated transport mechanisms, and structural engineering strategies that enable long-range, coherent, and tunable light guiding. This review has outlined how excitonic



interactions such as polariton formation, FRET, and RER underpin their unique propagation behaviors, and how rational design at the molecular, structural, and device levels has expanded their functionality across sensing, lasing, and optical logic. Together, these developments demonstrate that organic semiconductors are not merely lightweight alternatives to inorganic photonics but platforms with distinct capabilities arising from strong light–matter coupling at the molecular scale.

However, the path toward practical deployment is constrained by persistent challenges. Uniform fabrication of high-quality organic crystals remains difficult because non-covalent self-assembly is highly sensitive to fluctuations in the local environment, leading to stochastic nucleation and variability in orientation and morphology. Long-term operational stability of organic waveguides is further undermined by photooxidation, exciton–exciton annihilation, and thermally induced disorder, which progressively degrade quantum yield and increase propagation losses. Mitigation strategies such as polymer encapsulation, protective passivation layers, supramolecular locking, and hydrophobic coatings have shown promise, but their impact on scalability and device-level integration remains limited.<sup>67,89,94,95</sup> Integration with

external light sources and detectors, while advancing, continues to suffer from limited reproducibility, as deterministic positioning and precise alignment are still not routinely achieved. These issues underscore that the principles enabling efficient light emission are not, on their own, sufficient to guarantee reliable, manufacturable systems.

Looking forward, several domains appear particularly promising for active organic waveguides (Fig. 9). In biomedical technologies, their softness, biocompatibility, and ability to guide light with minimal bending loss offer advantages over passive structures, which require bulky optical couplers.<sup>151,152</sup> Exciton-mediated energy relay enables compact implantable platforms for continuous biosensing, glucose monitoring, neural recording, and minimally invasive diagnostics, where mechanical compliance and optical reliability are essential.<sup>153</sup>

In neuromorphic photonic computing, excitonic nonlinearities and reconfigurable propagation pathways suggest architectures that mimic synaptic plasticity, where identical hardware can be optically reprogrammed via pumping conditions.<sup>44,55</sup> Coupled with evanescent energy transfer between adjacent waveguides, these systems support dynamic connectivity, offering routes toward brain-inspired computation.<sup>154,155</sup> At the device level, the active nature of organic

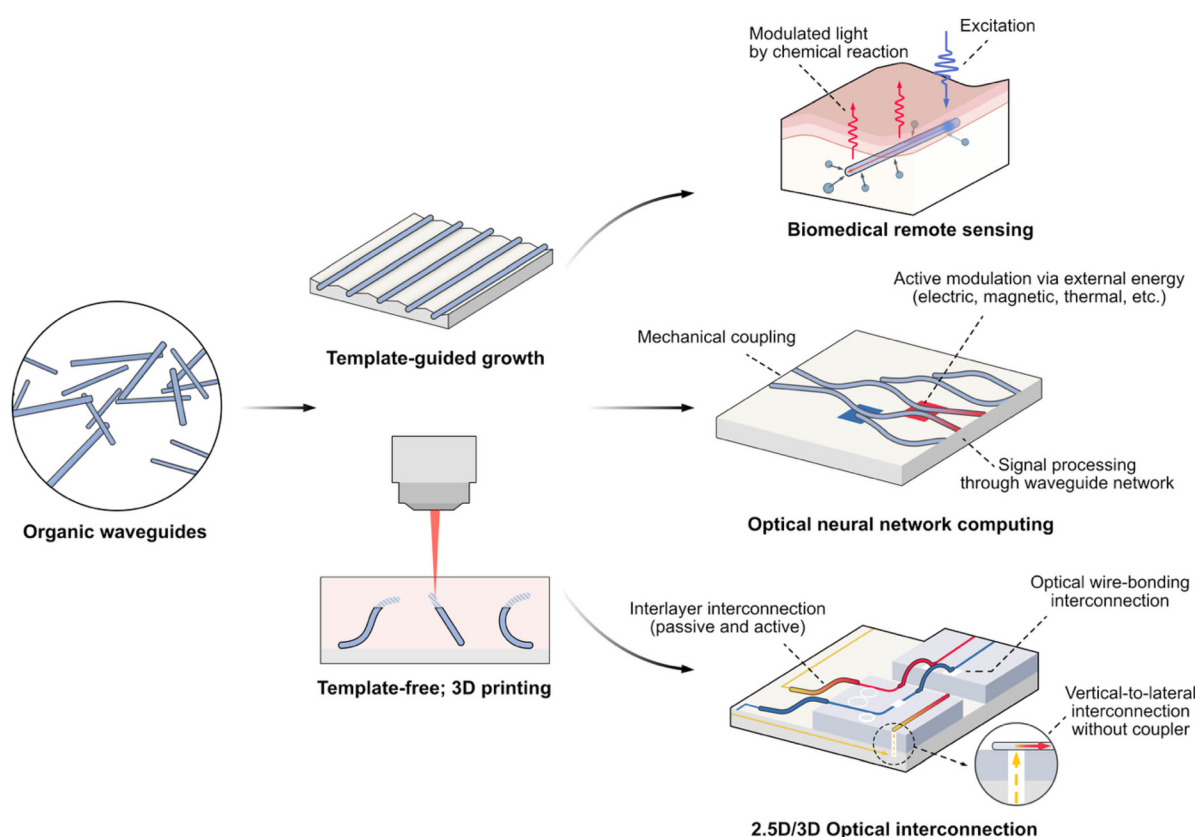


**FIG. 9.** Future perspective and emerging application fields of organic waveguides. The left column illustrates the present status of organic waveguide structures, which are typically fabricated in straight geometries that undergo physical shaping to enable reconfigurable architectures. The middle column represents advances in fabrication strategies, including template-guided growth and template-free 3D printing, which require further development to accommodate a broader range of materials. The right column highlights three key application fields driving future development: (top) Biomedical applications, particularly those involving remote sensing, optogenetic stimulation, and minimally invasive diagnostics; (middle) Artificial neural network computing, which leverages programmable optical routing and activation for neuromorphic architectures; (bottom) 2.5D/3D photonic integration, where mechanically reconfigurable waveguides enable vertical interconnects without bulky couplers.

waveguides allows modulation of light amplitude, phase, frequency, or polarization during propagation through external stimuli such as electric field.<sup>5</sup> These linear or nonlinear modulations enable essential computational functions such as weighted summation and thresholding to occur directly during optical propagation within the waveguide itself. This feature eliminates the need for separate computational components and enables dense waveguide networks for optical neural network computing.<sup>13,156–158</sup> Beyond these, optogenetics and biointerfaces represent natural applications, where organic waveguides could deliver light stimuli directly to biological tissues with reduced invasiveness and improved spatial precision.

Beyond neuromorphic and biointerfacing applications, active organic waveguides also offer distinct advantages for optical interconnection in densely packed photonic integrated circuits. Conventional systems rely on passive waveguides with coupling structures, such as micro-mirrors, grating couplers, or edge couplers, each demanding tight alignment tolerances and complex fabrication processing. These couplers introduce coupling losses, typically ranging from 0.5 to 3.0 dB per facet,<sup>159,160</sup> while lateral misalignments on the order of 0.5–3  $\mu\text{m}$  add an additional  $\sim 1$  dB loss.<sup>161</sup> Furthermore, these couplers consume large footprints, typically 300–1000  $\mu\text{m}$  tapers for edge coupling, and  $\sim 20 \times \sim 30 \mu\text{m}^2$  for grating couplers, thereby imposing a critical limit on areal density.

Organic active waveguides generate light internally, removing the need for such couplers and thereby enabling higher interconnect densities.<sup>116,162</sup> Typical organic waveguides have cross-sectional areas of 0.5–5  $\mu\text{m}^2$  and can be excited by localized spot illumination, efficiently converting out-of-plane excitation into guided in-plane modes. This internal light generation reduces the need for extended coupling structures and enables higher density interconnections.

Mechanical flexibility further enhances their integration density. Unlike rigid silicon platforms that require tapered couplers  $\sim 100 \mu\text{m}$  long to bridge vertical offsets as small as  $\sim 200 \text{ nm}$ ,<sup>163,164</sup> organic systems have demonstrated direct chip-to-chip interconnection across vertically separated layers.<sup>165</sup> Moreover, template-assisted growth techniques combined with intrinsic bending radii of  $\sim 10 \mu\text{m}$  allow organic waveguides to achieve conformal routing across vertical layers without bulky coupling structures.<sup>120,121</sup>

While propagation losses in organic active waveguides (0.000 27–1 dB/ $\mu\text{m}$ ) exceed those of Si-based waveguides (1–10 dB/m), such attenuation becomes less critical in high-density chip-to-chip interconnections, where optical paths are typically constrained to  $\mu\text{m}$ –mm scales.<sup>32,166–170</sup> In these short-range interconnects, coupling losses dominate the system performance rather than propagation losses. Thus, accounting for the external coupling, organic active waveguides can offer superior end-to-end efficiency.

Realizing these applications, however, depends critically on overcoming the fabrication bottlenecks that currently limit device-scale integration. Although self-assembly and template-guided growth have improved reliability through molecular- and structural-level control, these methods remain challenging for device-integrated fabrication and large-scale integration, which are essential for practical deployment.<sup>89,94,95</sup> Alternative approaches such as inkjet printing, transfer stamping, and two-photon lithography have emerged, showing early progress toward CMOS-compatible integration. However, these techniques remain largely limited to polymer systems rather than active crystalline materials. Establishing growth protocols that consistently deliver

large-area, defect-minimized, and directionally controlled structures is the most urgent bottleneck. Success here would enable multilayer (2.5D and 3D) interconnects that exploit the mechanical compliance of organic crystals for compact vertical coupling—an achievement difficult to realize with rigid silicon photonics.<sup>171</sup>

In conclusion, organic active waveguides stand at a transition point. Their exciton-driven transport, molecular tunability, and compatibility with soft and biological systems provide unique opportunities for applications that extend well beyond the reach of passive photonic platforms. However, their fragility, stochastic growth, and limited integration still pose formidable barriers. The future trajectory of the field will likely hinge on two converging thrusts: molecular-level stabilization strategies that reconcile efficiency with robustness, and deterministic, CMOS-compatible fabrication methods that enable scalable integration. Although these advances in material quality and reliability do not position organic waveguides to fully replace established inorganic platforms, they provide sufficient competitiveness in specific domains, particularly in applications operating over relatively short distances. Success along these directions would establish organic active waveguides not as experimental curiosities, but as indispensable components of next-generation photonic circuits, neuromorphic architectures, and bio-integrated optoelectronics.

## ACKNOWLEDGMENTS

This work was supported by the Air Force Office of Scientific Research Young Investigator Program (YIP) (Grant No. FA9550-23-1-0159; K.L.), Samsung Display Co. (Grant No. AWD-006596; K.L.), Industrial Strategic Technology Development Program (Grant No. 2410005219, Platform technology for enhanced OLED materials and device industry high-performance backplane and high-efficiency—J.K. and J.L.) funded by the Ministry of Trade, and the National Research Foundation of Korea (NRF) grant, funded by the Korea government (MSIT) (Grant No. RS-2024-00357783—D.H.P., RS-2025-24535263—J.K., and RS-2024-00463084—S.K., Y.B.), Basic Science Research Program through the National Research Foundation of Korea (NRF) funded by the Ministry of Education (Grant No. NRF-2022R1I1A1A01072213—S.K.), and the Korea Institute for Advancement of Technology (KIAT) grant (RS-2025-02263458—J.K.), Technology Innovation Program (RS-2025-02653941—J.K.), both funded by the Ministry of Trade, Industry & Energy (MOTIE, Korea).

## AUTHOR DECLARATIONS

### Conflict of Interest

The authors have no conflicts to disclose.

### Author Contributions

Do Wan Kim, Seokho Kim, Jinho Choi, Jaehyun Lee, Yongmin Baek, contributed equally to this paper.

**Do Wan Kim:** Writing – original draft (equal). **Seokho Kim:** Writing – original draft (equal). **Jinho Choi:** Writing – original draft (equal). **Jaehyun Lee:** Writing – original draft (equal). **Yongmin Baek:** Writing – original draft (equal). **Kyusang Lee:** Writing – review & editing (equal). **Dong Hyuk Park:** Writing – review & editing (equal). **Jongchan Kim:** Writing – review & editing (equal).

## DATA AVAILABILITY

Data sharing is not applicable to this article as no new data were created or analyzed in this study.

## REFERENCES

- <sup>1</sup>V. G. Kozlov, V. Bulović, P. E. Burrows, and S. R. Forrest, "Laser action in organic semiconductor waveguide and double-heterostructure devices," *Nature* **389**(6649), 362–364 (1997).
- <sup>2</sup>F. Balzer, V. G. Bordo, A. C. Simonsen, and H.-G. Rubahn, "Optical waveguiding in individual nanometer-scale organic fibers," *Phys. Rev. B* **67**(11), 115408 (2003).
- <sup>3</sup>Y. S. Zhao, J. Xu, A. Peng, H. Fu, Y. Ma, L. Jiang, and J. Yao, "Optical waveguide based on crystalline organic microtubes and microrods," *Angew. Chem. Int. Ed.* **47**(38), 7301–7305 (2008).
- <sup>4</sup>C. Zhang, J. Y. Zheng, Y. S. Zhao, and J. Yao, "Self-modulated white light out-coupling in doped organic nanowire waveguides via the fluctuations of singlet and triplet excitons during propagation," *Adv. Mater.* **23**(11), 1380–1384 (2011).
- <sup>5</sup>G. Zhao, H. Dong, Q. Liao, J. Jiang, Y. Luo, H. Fu, and W. Hu, "Organic field-effect optical waveguides," *Nat. Commun.* **9**(1), 4790 (2018).
- <sup>6</sup>Y. Yan, C. Zhang, J. Y. Zheng, J. Yao, and Y. S. Zhao, "Optical modulation based on direct photon-plasmon coupling in organic/metal nanowire heterojunctions," *Adv. Mater.* **24**(42), 5681–5686 (2012).
- <sup>7</sup>J. Y. Zheng, Y. Yan, X. Wang, Y. S. Zhao, J. Huang, and J. Yao, "Wire-on-wire growth of fluorescent organic heterojunctions," *J. Am. Chem. Soc.* **134**(6), 2880–2883 (2012).
- <sup>8</sup>S. Kim, C. Cui, J. Huang, H. Noh, D. H. Park, and D. J. Ahn, "Bio-photonic waveguides: Bio-photonic waveguide of a DNA-hybrid semiconductor prismatic hexagon," *Adv. Mater.* **32**(45), e2005238 (2020).
- <sup>9</sup>X. Yang, L. Lan, X. Pan, X. Liu, Y. Song, X. Yang, Q. Dong, L. Li, P. Naumov, and H. Zhang, "Electrically conductive hybrid organic crystals as flexible optical waveguides," *Nat. Commun.* **13**(1), 7874 (2022).
- <sup>10</sup>R. Huang, C. Wang, Y. Wang, and H. Zhang, "Elastic self-doping organic single crystals exhibiting flexible optical waveguide and amplified spontaneous emission," *Adv. Mater.* **30**(21), 1800814 (2018).
- <sup>11</sup>M.-P. Zhuo, J.-J. Wu, X.-D. Wang, Y.-C. Tao, Y. Yuan, and L.-S. Liao, "Hierarchical self-assembly of organic heterostructure nanowires," *Nat. Commun.* **10**(1), 3839 (2019).
- <sup>12</sup>L. Catalano, J. Berthaud, G. Dushaq, D. P. Karothu, R. Rezgui, M. Rasras, S. Ferlay, M. W. Hosseini, and P. Naumov, "Sequencing and welding of molecular single-crystal optical waveguides," *Adv. Funct. Mater.* **30**(35), 2003443 (2020).
- <sup>13</sup>A. V. Kumar, M. Rohullah, M. Chosenyah, G. Sindhuja, and R. Chandrasekar, "Hierarchical optical waveguides based on serpentine-like organic pseudoplastic crystals that mimic neural networks," *Angew. Chem. Int. Ed.* **64**(23), e202502122 (2025).
- <sup>14</sup>C. Zhang, Y. S. Zhao, and J. Yao, "Optical waveguides at micro/nanoscale based on functional small organic molecules," *Phys. Chem. Chem. Phys.* **13**(20), 9060–9073 (2011).
- <sup>15</sup>S. Chen, M.-P. Zhuo, X.-D. Wang, G.-Q. Wei, and L.-S. Liao, "Optical waveguides based on one-dimensional organic crystals," *Photonix* **2**(1), 2 (2021).
- <sup>16</sup>Q. Liao, H. Fu, and J. Yao, "Waveguide modulator by energy remote relay from binary organic crystalline microtubes," *Adv. Mater.* **21**(41), 4153–4157 (2009).
- <sup>17</sup>Y. Che, X. Yang, K. Balakrishnan, J. Zuo, and L. Zang, "Highly polarized and self-waveguided emission from single-crystalline organic nanobelts," *Chem. Mater.* **21**(13), 2930–2934 (2009).
- <sup>18</sup>H. Wang, Q. Liao, H. Fu, Y. Zeng, Z. Jiang, J. Ma, and J. Yao, "Ir(ppy)<sub>3</sub> phosphorescent microrods and nanowires: Promising micro-phosphors," *J. Mater. Chem.* **19**(1), 89–96 (2009).
- <sup>19</sup>Q. Bao, B. M. Goh, B. Yan, T. Yu, Z. Shen, and K. P. Loh, "Polarized emission and optical waveguide in crystalline perylene diimide microwires," *Adv. Mater.* **22**(33), 3661–3666 (2010).
- <sup>20</sup>S. Hayashi and T. Koizumi, "Elastic organic crystals of a fluorescent  $\pi$ -conjugated molecule," *Angew. Chem.* **128**(8), 2751–2754 (2016).
- <sup>21</sup>D. O'Carroll, I. Lieberwirth, and G. Redmond, "Melt-processed polyfluorene nanowires as active waveguides," *Small* **3**(7), 1178–1183 (2007).
- <sup>22</sup>K. Takazawa, J. Inoue, K. Mitsuishi, and T. Takamasu, "Fraction of a millimeter propagation of exciton polaritons in photoexcited nanofibers of organic dye," *Phys. Rev. Lett.* **105**(6), 067401 (2010).
- <sup>23</sup>Y. Yan and Y. S. Zhao, "Exciton polaritons in 1D organic nanocrystals," *Adv. Funct. Mater.* **22**(7), 1330–1332 (2012).
- <sup>24</sup>E. H. Cho, B. Kim, S. Jun, J. Lee, D. H. Park, K. Lee, J. Kim, J. Kim, and J. Joo, "Remote biosensing with polychromatic optical waveguide using blue light-emitting organic nanowires hybridized with quantum dots," *Adv. Funct. Mater.* **24**(24), 3684–3691 (2014).
- <sup>25</sup>K. Takazawa, Y. Kitahama, Y. Kimura, and G. Kido, "Optical waveguide self-assembled from organic dye molecules in solution," *Nano Lett.* **5**(7), 1293–1296 (2005).
- <sup>26</sup>D. O'Carroll and G. Redmond, "Polyfluorene nanowire active waveguides as sub-wavelength polarized light sources," *Phys. E* **40**(7), 2468–2473 (2008).
- <sup>27</sup>Q. H. Cui, Y. S. Zhao, and J. Yao, "Photonic applications of one-dimensional organic single-crystalline nanostructures: Optical waveguides and optically pumped lasers," *J. Mater. Chem.* **22**(10), 4136–4140 (2012).
- <sup>28</sup>W. Zhu, R. Zheng, Y. Zhen, Z. Yu, H. Dong, H. Fu, Q. Shi, and W. Hu, "Rational design of charge-transfer interactions in halogen-bonded co-crystals toward versatile solid-state optoelectronics," *J. Am. Chem. Soc.* **137**(34), 11038–11046 (2015).
- <sup>29</sup>W. Zhu, R. Zheng, X. Fu, H. Fu, Q. Shi, Y. Zhen, H. Dong, and W. Hu, "Revealing the charge-transfer interactions in self-assembled organic cocrystals: Two-dimensional photonic applications," *Angew. Chem. Int. Ed.* **54**(23), 6785–6789 (2015).
- <sup>30</sup>S. Hayashi, S. Yamamoto, D. Takeuchi, Y. Ie, and K. Takagi, "Creating elastic organic crystals of  $\pi$ -conjugated molecules with bending mechanofluorochromism and flexible optical waveguide," *Angew. Chem. Int. Ed.* **57**(52), 17002–17008 (2018).
- <sup>31</sup>M. Annadhasan, S. Basak, N. Chandrasekhar, and R. Chandrasekar, "Next-generation organic photonics: The emergence of flexible crystal optical waveguides," *Adv. Opt. Mater.* **8**(21), 2000959 (2020).
- <sup>32</sup>D. Tian and Y. Chen, "Optical waveguides in organic crystals of polycyclic arenes," *Adv. Opt. Mater.* **9**(23), 2002264 (2021).
- <sup>33</sup>M.-C. Choi, J. Wakita, C.-S. Ha, and S. Ando, "Highly transparent and refractive polyimides with controlled molecular structure by chlorine side groups," *Macromolecules* **42**(14), 5112–5120 (2009).
- <sup>34</sup>N. Chandrasekhar, M. A. Mohiddon, and R. Chandrasekar, "Organic submicro tubular optical waveguides: Self-assembly, diverse geometries, efficiency, and remote sensing properties," *Adv. Opt. Mater.* **1**(4), 305–311 (2013).
- <sup>35</sup>P. K. Tapaswi, M.-C. Choi, K.-M. Jeong, S. Ando, and C.-S. Ha, "Transparent aromatic polyimides derived from thiophenyl-substituted benzidines with high refractive index and small birefringence," *Macromolecules* **48**(11), 3462–3474 (2015).
- <sup>36</sup>D. W. Kim, J. Kim, Y. Baek, K. Choi, J. Kim, S. H. Yoo, J. Song, J. Choi, H. Noh, K. Lee, J.-W. Jang, and D. H. Park, "Rapidly grown hexagonal organic microtubes using ionic liquids for an enhanced optical waveguide effect," *Adv. Opt. Mater.* **12**(22), 2303077 (2024).
- <sup>37</sup>M. Hertzog, M. Wang, J. Mony, and K. Börjesson, "Strong light-matter interactions: A new direction within chemistry," *Chem. Soc. Rev.* **48**(3), 937–961 (2019).
- <sup>38</sup>M.-P. Zhuo, X.-D. Wang, and L.-S. Liao, "Construction and optoelectronic applications of organic core/shell micro/nanostructures," *Mater. Horiz.* **7**(12), 3161–3175 (2020).
- <sup>39</sup>Y.-L. Shi, Q. Lv, Y.-C. Tao, Y.-X. Ma, and X.-D. Wang, "Design and growth of branched organic crystals: Recent advances and future applications," *Angew. Chem. Int. Ed.* **61**(40), e202208768 (2022).
- <sup>40</sup>Y.-X. Ma, J. Yang, S.-H. Chen, H.-T. Lin, C.-C. Yan, S.-P. Zhuo, and X.-D. Wang, "Organic low-dimensional heterojunctions toward future applications," *Matter* **5**(11), 3706–3739 (2022).
- <sup>41</sup>Q. Lv, X.-D. Wang, and L.-S. Liao, "Exploring axial organic multiblock heterostructure nanowires: Advances in molecular design, synthesis, and functional applications," *Adv. Funct. Mater.* **32**(28), 2202364 (2022).
- <sup>42</sup>M. Godumala, A. V. Kumar, and R. Chandrasekar, "Room-temperature phosphorescent organic materials for optical waveguides," *J. Mater. Chem. C* **9**(40), 14115–14132 (2021).



- <sup>43</sup>N. Chandrasekhar and R. Chandrasekar, "Engineering self-assembled fluorescent organic nanotapes and submicrotubes from  $\pi$ -conjugated molecules," *Chem. Commun.* **46**(17), 2915 (2010).
- <sup>44</sup>N. Chandrasekhar and R. Chandrasekar, "Reversibly shape-shifting organic optical waveguides: Formation of organic nanorings, nanotubes, and nanosheets," *Angew. Chem. Int. Ed.* **51**(15), 3556 (2012).
- <sup>45</sup>S. Basak and R. Chandrasekar, "Passive optical waveguiding organic rectangular tubes: Tube cutting, controlling light propagation distance and multiple optical out-puts," *J. Mater. Chem. C* **2**(8), 1404–1408 (2014).
- <sup>46</sup>X. Wang, Y. Zhou, T. Lei, N. Hu, E.-Q. Chen, and J. Pei, "Structural–property relationship in pyrazino[2,3-*g*]quinoxaline derivatives: Morphology, photophysical, and waveguide properties," *Chem. Mater.* **22**(12), 3735–3745 (2010).
- <sup>47</sup>W. Hu, Y. Chen, H. Jiang, J. Li, G. Zou, Q. Zhang, D. Zhang, P. Wang, and H. Ming, "Optical waveguide based on a polarized polydiacetylene microtube," *Adv. Mater.* **26**(19), 3136–3141 (2014).
- <sup>48</sup>K. Takazawa, J. Inoue, and K. Mitsuishi, "Optical microring resonators constructed from organic dye nanofibers and their application to miniaturized channel drop/add filters," *ACS Appl. Mater. Interfaces* **5**(13), 6182–6188 (2013).
- <sup>49</sup>J.-Y. Zheng, H. Xu, J. J. Wang, S. Winters, C. Motta, E. Karademir, W. Zhu, E. Varila, G. S. Duesberg, S. Sanvito, W. Hu, and J. F. Donegan, "Vertical single-crystalline organic nanowires on graphene: Solution-phase epitaxy and optical microcavities," *Nano Lett.* **16**(8), 4754–4762 (2016).
- <sup>50</sup>S. Hou, M. Khatoniari, K. Ding, Y. Qu, A. Napolov, V. M. Menon, and S. R. Forrest, "Ultralong-range energy transport in a disordered organic semiconductor at room temperature via coherent exciton-polariton propagation," *Adv. Mater.* **32**(28), 2002127 (2020).
- <sup>51</sup>Q. Liao, Z. Xu, X. Zhong, W. Dang, Q. Shi, C. Zhang, Y. Weng, Z. Li, and H. Fu, "An organic nanowire waveguide exciton-polariton sub-microlaser and its photonic application," *J. Mater. Chem. C* **2**(15), 2773–2778 (2014).
- <sup>52</sup>A. R. Clapp, I. L. Medintz, and H. Mattoussi, "Förster resonance energy transfer investigations using quantum-dot fluorophores," *ChemPhysChem* **7**(1), 47–57 (2006).
- <sup>53</sup>K. Takazawa, "Flexibility and bending loss of waveguiding molecular fibers self-assembled from thianthrene dye," *Chem. Phys. Lett.* **452**(1), 168–172 (2008).
- <sup>54</sup>K. Takazawa, J. Inoue, K. Mitsuishi, and T. Takamasu, "Micrometer-scale photonic circuit components based on propagation of exciton polaritons in organic dye nanofibers," *Adv. Mater.* **23**(32), 3659–3663 (2011).
- <sup>55</sup>C. Zhang, C.-L. Zou, H. Dong, Y. Yan, J. Yao, and Y. S. Zhao, "Dual-color single-mode lasing in axially coupled organic nanowire resonators," *Sci. Adv.* **3**(7), e1700225 (2017).
- <sup>56</sup>Q. H. Cui, Q. Peng, Y. Luo, Y. Jiang, Y. Yan, C. Wei, Z. Shuai, C. Sun, J. Yao, and Y. S. Zhao, "Asymmetric photon transport in organic semiconductor nanowires through electrically controlled exciton diffusion," *Sci. Adv.* **4**(3), eaap9861 (2018).
- <sup>57</sup>T. Förster, "Zwischenmolekulare Energiewanderung und Fluoreszenz," *Ann. Phys.* **437**(1–2), 55–75 (1948).
- <sup>58</sup>T. Matsuo, K. Ikeda, and S. Hayashi, "Flexible Förster resonance energy transfer-assisted optical waveguide based on elastic mixed molecular crystals," *Aggregate* **4**(6), e378 (2023).
- <sup>59</sup>K. E. Sapsford, L. Berti, and I. L. Medintz, "Materials for fluorescence resonance energy transfer analysis: Beyond traditional donor-acceptor combinations," *Angew. Chem. Int. Ed.* **45**(28), 4562–4589 (2006).
- <sup>60</sup>K. C. Kao and G. A. Hockham, "Dielectric-fibre surface waveguides for optical frequencies," *Proc. Inst. Electr. Eng.* **113**(7), 1151–1158 (1966).
- <sup>61</sup>H. Ma, A. K.-Y. Jen, and L. R. Dalton, "Polymer-based optical waveguides: Materials, processing, and devices," *Adv. Mater.* **14**(19), 1339–1365 (2002).
- <sup>62</sup>R. G. Hunsperger, "Losses in optical waveguides," in *Integrated Optics: Theory and Technology*, edited by R. G. Hunsperger (Springer, New York, NY, 2009), pp. 107–128.
- <sup>63</sup>E. Podda, M. Arca, A. Pintus, V. Lippolis, S. J. Coles, J. B. Orton, S. Porcu, P. C. Ricci, and M. C. Aragoni, "Ultra-low optical loss in single crystal waveguides of fluorene/fluorenone Cd<sup>II</sup> coordination polymers," *JACS Au* **5**(2), 727–739 (2025).
- <sup>64</sup>G. M. Akselrod, Y. R. Tischler, E. R. Young, D. G. Nocera, and V. Bulovic, "Exciton-exciton annihilation in organic polariton microcavities," *Phys. Rev. B* **82**(11), 113106 (2010).
- <sup>65</sup>J. M. Hodgkiss, S. Albert-Seifried, A. Rao, A. J. Barker, A. R. Campbell, R. A. Marsh, and R. H. Friend, "Exciton-charge annihilation in organic semiconductor films," *Adv. Funct. Mater.* **22**(8), 1567–1577 (2012).
- <sup>66</sup>D. Barman, M. Annadhasan, A. P. Bidkar, P. Rajamalli, D. Barman, S. S. Ghosh, R. Chandrasekar, and P. K. Iyer, "Highly efficient color-tunable organic co-crystals unveiling polymorphism, isomerism, delayed fluorescence for optical waveguides and cell-imaging," *Nat. Commun.* **14**(1), 6648 (2023).
- <sup>67</sup>Y. Yu, X.-Y. Xia, C.-F. Xu, Z.-J. Lv, X.-D. Wang, and L.-S. Liao, "Customizable organic charge-transfer cocrystals for the dual-mode optoelectronics in the NIR (II) window," *J. Am. Chem. Soc.* **146**(17), 11845–11854 (2024).
- <sup>68</sup>J. Lagois, "Depth-dependent eigenenergies and damping of excitonic polaritons near a semiconductor surface," *Phys. Rev. B* **23**(10), 5511–5520 (1981).
- <sup>69</sup>J. Tang, J. Zhang, Y. Lv, H. Wang, F. F. Xu, C. Zhang, L. Sun, J. Yao, and Y. S. Zhao, "Room temperature exciton-polariton Bose-Einstein condensation in organic single-crystal microribbon cavities," *Nat. Commun.* **12**(1), 3265 (2021).
- <sup>70</sup>Z. Jiang, A. Ren, Y. Yan, J. Yao, and Y. S. Zhao, "Exciton-polaritons and their Bose-Einstein condensates in organic semiconductor microcavities," *Adv. Mater.* **34**(4), 2106095 (2022).
- <sup>71</sup>S. Kéna-Cohen and S. R. Forrest, "Room-temperature polariton lasing in an organic single-crystal microcavity," *Nat. Photonics* **4**(6), 371–375 (2010).
- <sup>72</sup>T. Byrnes, N. Y. Kim, and Y. Yamamoto, "Exciton-polariton condensates," *Nat. Phys.* **10**(11), 803–813 (2014).
- <sup>73</sup>A. V. Kavokin, J. J. Baumberg, G. Malpuech, and F. P. Laussy, *Microcavities* (Oxford University Press, 2017).
- <sup>74</sup>B. Liu, J. Horowitz, and S. R. Forrest, "Guided Bloch surface wave polaritons on patterned distributed Bragg reflectors at room temperature," *ACS Photonics* **10**(12), 4476–4482 (2023).
- <sup>75</sup>T. L. Penner, H. R. Motschmann, N. J. Armstrong, M. C. Ezenyilimba, and D. J. Williams, "Efficient phase-matched second-harmonic generation of blue light in an organic waveguide," *Nature* **367**(6458), 49–51 (1994).
- <sup>76</sup>N. Mitetelo, D. Venkatakrishnarao, J. Ravi, M. Popov, E. Mamonov, T. V. Murzina, and R. Chandrasekar, "Chirality-controlled multiphoton luminescence and second-harmonic generation from enantiomeric organic micro-optical waveguides," *Adv. Opt. Mater.* **7**(11), 1801775 (2019).
- <sup>77</sup>M. Shimizu, Y. Takeda, M. Higashi, and T. Hiyama, "1,4-bis(alkenyl)-2,5-dipiperidinobenzenes: Minimal fluorophores exhibiting highly efficient emission in the solid state," *Angew. Chem. Int. Ed.* **48**(20), 3653–3656 (2009).
- <sup>78</sup>Y. Hong, J. W. Y. Lam, and B. Z. Tang, "Aggregation-induced emission," *Chem. Soc. Rev.* **40**(11), 5361 (2011).
- <sup>79</sup>S. Abou-Hatab, V. A. Spata, and S. Matsika, "Substituent effects on the absorption and fluorescence properties of anthracene," *J. Phys. Chem. A* **121**(6), 1213–1222 (2017).
- <sup>80</sup>B. Shao, H. Qian, Q. Li, and I. Aprahamian, "Structure property analysis of the solution and solid-state properties of bistable photochromic hydrazones," *J. Am. Chem. Soc.* **141**(20), 8364–8371 (2019).
- <sup>81</sup>E. Cho, J. Choi, S. Jo, D. Park, Y. K. Hong, D. Kim, and T. S. Lee, "A single-benzene-based fluorophore: Optical waveguiding in the crystal form," *ChemPlusChem* **84**(8), 1130–1134 (2019).
- <sup>82</sup>Y. Yuan, G. Giri, A. L. Ayzner, A. P. Zoombelt, S. C. B. Mannsfeld, J. Chen, D. Nordlund, M. F. Toney, J. Huang, and Z. Bao, "Ultra-high mobility transparent organic thin film transistors grown by an off-centre spin-coating method," *Nat. Commun.* **5**(1), 3005 (2014).
- <sup>83</sup>S. Hotta and T. Yamao, "The thiophene/phenylene co-oligomers: Exotic molecular semiconductors integrating high-performance electronic and optical functionalities," *J. Mater. Chem.* **21**(5), 1295–1304 (2011).
- <sup>84</sup>H. Liu, Z. Lu, Z. Zhang, Y. Wang, and H. Zhang, "Highly elastic organic crystals for flexible optical waveguides," *Angew. Chem. Int. Ed.* **57**(28), 8448–8452 (2018).
- <sup>85</sup>Y.-C. Lu, Y.-T. Hsu, T.-Y. Yang, I.-C. Liou, S.-W. Wang, P.-C. Huang, J.-J. Lee, L.-L. Lai, and H.-F. Hsu, "Converting non-mesogenic to mesogenic stacking of amino-s-triazine-based dendrons with p-CN phenyl unit by eliminating peripheral dipole," *Nanomaterials* **12**(2), 185 (2022).
- <sup>86</sup>M.-H. Yen, J. Chairapra, X. Zeng, Y. Liu, L. Cseh, G. H. Mehl, and G. Ungar, "Added alkane allows thermal thinning of supramolecular columns by forming superlattice—An x-ray and neutron study," *J. Am. Chem. Soc.* **138**(18), 5757–5760 (2016).



- <sup>87</sup>J. Chen, Y. Cao, A. Joy, J. Li, T. Hao, J. Huang, X. Li, F. Liu, and H. Xie, "Dynamic dipole moment of luminescent liquid crystals enabled highly efficient active waveguide materials design and synthesis," *Adv. Opt. Mater.* **12**(25), 2400726 (2024).
- <sup>88</sup>B. Lu, X. Fang, and D. Yan, "Luminescent polymorphic co-crystals: A promising way to the diversity of molecular assembly, fluorescence polarization, and optical waveguide," *ACS Appl. Mater. Interfaces* **12**(28), 31940–31951 (2020).
- <sup>89</sup>A. Navarro-Huerta, T. Matsuo, A. S. Mikherdov, J. Blahut, E. Bartůňková, P. Jiang, M. Dračinský, S. Teat, M. Jin, S. Hayashi, and B. Rodríguez-Molina, "Optical waveguiding charge-transfer cocrystals: Examining the impact of molecular rotations on their photoluminescence," *J. Am. Chem. Soc.* **147**(10), 8343–8349 (2025).
- <sup>90</sup>X. Xia, Q. Lv, C. Xu, Y. Yu, L. Wang, X. Wang, and L. Liao, "Crafting near-infrared photonics via the programmable assembly of organic heterostructures at multiscale level," *Adv. Funct. Mater.* **34**(24), 2312478 (2024).
- <sup>91</sup>G. R. Ferreira, B. Nowacki, A. Magalhães, E. R. deAzevedo, E. L. De Sá, L. C. Akcelrud, and R. F. Bianchi, "Controlling photo-oxidation processes of a poly-fluorene derivative: The effect of additives and mechanism," *Mater. Chem. Phys.* **146**(3), 212–217 (2014).
- <sup>92</sup>F. So and D. Kondakov, "Degradation mechanisms in small-molecule and polymer organic light-emitting diodes," *Adv. Mater.* **22**(34), 3762–3777 (2010).
- <sup>93</sup>H. Zhang, D. Lin, W. Liu, Y. Wang, Z. Li, D. Jin, J. Wang, X. Zhang, L. Huang, S. Wang, C. Xu, Y. Kan, and L. Xie, "Crystallization-enhanced stability by effectively suppressing photooxidation defect for optoelectronic devices," *Adv. Mater. Inter.* **9**(15), 2200194 (2022).
- <sup>94</sup>J.-C. Christopherson, F. Topić, C. J. Barrett, and T. Frišić, "Halogen-bonded cocrystals as optical materials: Next-generation control over light-matter interactions," *Cryst. Growth Des.* **18**(2), 1245–1259 (2018).
- <sup>95</sup>M. Zhuo, Y. Tao, X. Wang, Y. Wu, S. Chen, L. Liao, and L. Jiang, "2D organic photonics: An asymmetric optical waveguide in self-assembled halogen-bonded cocrystals," *Angew. Chem.* **130**(35), 11470–11474 (2018).
- <sup>96</sup>J. Ravi, T. Feiler, A. Mondal, A. A. L. Michalchuk, C. M. Reddy, B. Bhattacharya, F. Emmerling, and R. Chandrasekar, "Plastically bendable organic crystals for monolithic and hybrid micro-optical circuits," *Adv. Opt. Mater.* **11**(13), 2201518 (2023).
- <sup>97</sup>H. Lin, Y. Ma, S. Chen, and X. Wang, "Hierarchical integration of organic core/shell microwires for advanced photonics," *Angew. Chem. Int. Ed.* **62**(2), e202214214 (2023).
- <sup>98</sup>L. Zhou, S. Dodd, C. Capacci-Daniel, S. Garad, R. Panicucci, and V. Sethuraman, "Co-crystal formation based on structural matching," *Eur. J. Pharm. Sci.* **88**, 191–201 (2016).
- <sup>99</sup>W. Z. Yuan, P. Lu, S. Chen, J. W. Y. Lam, Z. Wang, Y. Liu, H. S. Kwok, Y. Ma, and B. Z. Tang, "Changing the behavior of chromophores from aggregation-caused quenching to aggregation-induced emission: Development of highly efficient light emitters in the solid state," *Adv. Mater.* **22**(19), 2159–2163 (2010).
- <sup>100</sup>Q. Li, Y. Jia, L. Dai, Y. Yang, and J. Li, "Controlled rod nanostructured assembly of diphenylalanine and their optical waveguide properties," *ACS Nano* **9**(3), 2689–2695 (2015).
- <sup>101</sup>M. Pan, Y. Zhu, K. Wu, L. Chen, Y. Hou, S. Yin, H. Wang, Y. Fan, and C. Su, "Epitaxial growth of hetero-Ln-MOF hierarchical single crystals for domain- and orientation-controlled multicolor luminescence 3D coding capability," *Angew. Chem. Int. Ed.* **56**(46), 14582–14586 (2017).
- <sup>102</sup>C. Zhang, Y. Yan, Y. Jing, Q. Shi, Y. S. Zhao, and J. Yao, "One-dimensional organic photonic heterostructures: Rational construction and spatial engineering of excitonic emission," *Adv. Mater.* **24**(13), 1703–1708 (2012).
- <sup>103</sup>M.-J. Sun, Y. Liu, Y. Yan, R. Li, Q. Shi, Y. S. Zhao, Y.-W. Zhong, and J. Yao, "In situ visualization of assembly and photonic signal processing in a triplet light-harvesting nanosystem," *J. Am. Chem. Soc.* **140**(12), 4269–4278 (2018).
- <sup>104</sup>Q. Zhao, H. Lai, H. Chen, H. Li, and F. He, "H- and J-aggregation inspiring efficient solar conversion," *J. Mater. Chem. A* **9**(2), 1119–1126 (2021).
- <sup>105</sup>N. S. Sariciftci, D. Braun, C. Zhang, V. I. Srdanov, A. J. Heeger, G. Stucky, and F. Wudl, "Semiconducting polymer-buckminsterfullerene heterojunctions: Diodes, photodiodes, and photovoltaic cells," *Appl. Phys. Lett.* **62**(6), 585–587 (1993).
- <sup>106</sup>Q.-X. Chen, Y.-Y. Lu, Y. Yang, L.-G. Chang, Y. Li, Y. Yang, Z. He, J.-W. Liu, Y. Ni, and S.-H. Yu, "Stress-induced ordering evolution of 1D segmented heteronanostructures and their chemical post-transformations," *Nat. Commun.* **15**(1), 3208 (2024).
- <sup>107</sup>Q. Lv, X.-D. Wang, Y. Yu, M.-P. Zhuo, M. Zheng, and L.-S. Liao, "Lattice-mismatch-free growth of organic heterostructure nanowires from cocrystals to alloys," *Nat. Commun.* **13**(1), 3099 (2022).
- <sup>108</sup>M.-P. Zhuo, X. Wei, Y.-Y. Li, Y.-L. Shi, G.-P. He, H. Su, K.-Q. Zhang, J.-P. Guan, X.-D. Wang, Y. Wu, and L.-S. Liao, "Visualizing the interfacial-layer-based epitaxial growth process toward organic core-shell architectures," *Nat. Commun.* **15**(1), 1130 (2024).
- <sup>109</sup>Y. Shi, Q. Lv, Y. Tao, Y. Ma, and X. Wang, "Design and growth of branched organic crystals: Recent advances and future applications," *Angew. Chem.* **134**(40), e202208768 (2022).
- <sup>110</sup>Z. Qi, Y. Ma, and D. Yan, "One-dimensional molecular co-crystal alloys capable of full-color emission for low-loss optical waveguide and optical logic gate," *Aggregate* **5**(1), e411 (2024).
- <sup>111</sup>C. Zhang, Y. Yan, J. Yao, and Y. S. Zhao, "Manipulation of light flows in organic color-graded microstructures towards integrated photonic heterojunction devices," *Adv. Mater.* **25**(20), 2854–2859 (2013).
- <sup>112</sup>H. Gao, Y. Qiu, J. Feng, S. Li, H. Wang, Y. Zhao, X. Wei, X. Jiang, Y. Su, Y. Wu, and L. Jiang, "Nano-confined crystallization of organic ultrathin nanostructure arrays with programmable geometries," *Nat. Commun.* **10**(1), 3912 (2019).
- <sup>113</sup>J. Feng, X. Jiang, X. Yan, Y. Wu, B. Su, H. Fu, J. Yao, and L. Jiang, "Capillary-bridge lithography for patterning organic crystals toward mode-tunable micro-laser arrays," *Adv. Mater.* **29**(1), 1603652 (2017).
- <sup>114</sup>I. G. Lezama, M. Nakano, N. A. Minder, Z. Chen, F. V. Di Girolamo, A. Facchetti, and A. F. Morpurgo, "Single-crystal organic charge-transfer interfaces probed using Schottky-gated heterostructures," *Nat. Mater.* **11**(9), 788–794 (2012).
- <sup>115</sup>Z. Qin, C. Gao, H. Gao, T. Wang, H. Dong, and W. Hu, "Molecular doped, color-tunable, high-mobility, emissive, organic semiconductors for light-emitting transistors," *Sci. Adv.* **8**(27), eabp8775 (2022).
- <sup>116</sup>R. B. Taylor, P. E. Burrows, and S. R. Forrest, "An integrated, crystalline organic waveguide-coupled InGaAs photodetector," *IEEE Photonics Technol. Lett.* **9**(3), 365–367 (1997).
- <sup>117</sup>C.-F. Xu, W.-Y. Yang, Q. Lv, X.-D. Wang, and L.-S. Liao, "Directed self-assembly of organic crystals into chip-like heterostructures for signal processing," *Sci. China Mater.* **66**(2), 733–739 (2023).
- <sup>118</sup>Y. Qiu, B. Zhang, J. Yang, H. Gao, S. Li, L. Wang, P. Wu, Y. Su, Y. Zhao, J. Feng, L. Jiang, and Y. Wu, "Wafer-scale integration of stretchable semiconducting polymer microstructures via capillary gradient," *Nat. Commun.* **12**(1), 7038 (2021).
- <sup>119</sup>X. Xia, L. Ding, Q. Lv, X. Wang, and L. Liao, "Vapor-phase growth strategies of fabricating organic crystals for optoelectronic applications," *Adv. Elect. Mater.* **8**(12), 2200753 (2022).
- <sup>120</sup>Y. Wu, J. Feng, X. Jiang, Z. Zhang, X. Wang, B. Su, and L. Jiang, "Positioning and joining of organic single-crystalline wires," *Nat. Commun.* **6**(1), 6737 (2015).
- <sup>121</sup>J. Song, X. Wang, J. Liao, W. Zhou, J. Song, Z. Zhao, L. Zhang, E. Joselevich, and J. Xu, "Horizontally-oriented growth of organic crystalline nanowires on polymer films for in-situ flexible photodetectors with vis-NIR response and high bending stability," *Adv. Funct. Mater.* **33**(15), 2213888 (2023).
- <sup>122</sup>M. Zou, C. Liao, S. Liu, C. Xiong, C. Zhao, J. Zhao, Z. Gan, Y. Chen, K. Yang, D. Liu, Y. Wang, and Y. Wang, "Fiber-tip polymer clamped-beam probe for high-sensitivity nanoforce measurements," *Light Sci. Appl.* **10**(1), 171 (2021).
- <sup>123</sup>F. Van Schoonhoven, Y. Tomishige, A. Abazi, A. Sánchez-Postigo, J. Chen, Y. Mikami, N. Tate, Y. Oki, C. Schuck, and H. Yoshioka, "Inkjet-printed waveguide-coupled passive wedge-shaped microdisk resonator with refractive index tunability," *Opt. Mater. Express* **14**(7), 1767 (2024).
- <sup>124</sup>X. Shang, N. Wang, S. Cao, H. Chen, D. Fan, N. Zhou, and M. Qiu, "Fiber-integrated force sensor using 3D printed spring-composed fabry-perot cavities with a high precision down to tens of piconewton," *Adv. Mater.* **36**(2), 2305121 (2024).
- <sup>125</sup>D. Zhu, S. Jiang, Y. Wang, D. Liu, W. Bao, L. Liu, J. Qu, Y. Wang, and C. Liao, "Ultrafast laser 3D nanolithography of organic-inorganic hybrid waveguide devices," *APL Photonics* **10**(2), 026101 (2025).

- <sup>126</sup>A. Grabulosa, J. Moughames, X. Porte, M. Kadic, and D. Brunner, "Additive 3D photonic integration that is CMOS compatible," *Nanotechnology* **34**(32), 322002 (2023).
- <sup>127</sup>J. Y. Zheng, Y. Yan, X. Wang, W. Shi, H. Ma, Y. S. Zhao, and J. Yao, "Hydrogen peroxide vapor sensing with organic core/sheath nanowire optical waveguides," *Adv. Mater.* **24**(35), OP194–OP199 (2012).
- <sup>128</sup>M. S. Kwon, D. Lee, S. Seo, J. Jung, and J. Kim, "Tailoring intermolecular interactions for efficient room-temperature phosphorescence from purely organic materials in amorphous polymer matrices," *Angew. Chem.* **126**(42), 11359–11363 (2014).
- <sup>129</sup>Q. Li, H. Gao, J. Gu, Z. Zhang, G. Liang, H. Liu, and S. Qiao, "Design and optical waveguide behavior of full-color emitting materials with adjustable band gap," *Org. Electron.* **125**, 106954 (2024).
- <sup>130</sup>W. H. Jung, J. H. Park, S. Kim, C. Cui, and D. J. Ahn, "Molecular doping of nucleic acids into light emitting crystals driven by multisite-intermolecular interaction," *Nat. Commun.* **13**(1), 6193 (2022).
- <sup>131</sup>S. H. Back, J. H. Park, C. Cui, and D. J. Ahn, "Bio-recognitive photonics of a DNA-guided organic semiconductor," *Nat. Commun.* **7**(1), 10234 (2016).
- <sup>132</sup>L. Lan, X. Yang, B. Tang, X. Yu, X. Liu, L. Li, P. Naumov, and H. Zhang, "Hybrid elastic organic crystals that respond to aerial humidity," *Angew. Chem. Int. Ed.* **61**(14), e202200196 (2022).
- <sup>133</sup>Q. Di, L. Li, X. Miao, L. Lan, X. Yu, B. Liu, Y. Yi, P. Naumov, and H. Zhang, "Fluorescence-based thermal sensing with elastic organic crystals," *Nat. Commun.* **13**(1), 5280 (2022).
- <sup>134</sup>W. Zhang, J. Yao, and Y. S. Zhao, "Organic micro/nanoscale lasers," *Acc. Chem. Res.* **49**(9), 1691–1700 (2016).
- <sup>135</sup>J. Gierschner, S. Varghese, and S. Y. Park, "Organic single crystal lasers: A materials view," *Adv. Opt. Mater.* **4**(3), 348–364 (2016).
- <sup>136</sup>D. O'Carroll, I. Lieberwirth, and G. Redmond, "Microcavity effects and optically pumped lasing in single conjugated polymer nanowires," *Nat. Nanotechnol.* **2**(3), 180–184 (2007).
- <sup>137</sup>X. Wang, Z. Li, M. Zhuo, Y. Wu, S. Chen, J. Yao, and H. Fu, "Tunable near-infrared organic nanowire nanolasers," *Adv. Funct. Mater.* **27**(45), 1703470 (2017).
- <sup>138</sup>Z. Yu, Y. Wu, Q. Liao, H. Zhang, S. Bai, H. Li, Z. Xu, C. Sun, X. Wang, J. Yao, and H. Fu, "Self-assembled microdisk lasers of perylenediimides," *J. Am. Chem. Soc.* **137**(48), 15105–15111 (2015).
- <sup>139</sup>X. Wang, Q. Liao, H. Li, S. Bai, Y. Wu, X. Lu, H. Hu, Q. Shi, and H. Fu, "Near-infrared lasing from small-molecule organic hemispheres," *J. Am. Chem. Soc.* **137**(29), 9289–9295 (2015).
- <sup>140</sup>S. Kushida, D. Okada, F. Sasaki, Z. Lin, J. Huang, and Y. Yamamoto, "Low-threshold whispering gallery mode lasing from self-assembled microspheres of single-sort conjugated polymers," *Adv. Opt. Mater.* **5**(10), 1700123 (2017).
- <sup>141</sup>Y. S. Zhao, A. Peng, H. Fu, Y. Ma, and J. Yao, "Nanowire waveguides and ultraviolet lasers based on small organic molecules," *Adv. Mater.* **20**(9), 1661–1665 (2008).
- <sup>142</sup>Y. Tao, S. Peng, X. Wang, Z. Li, X. Zhang, and L. Liao, "Sequential self-assembly of 1D branched organic homostructures with optical logic gate function," *Adv. Funct. Mater.* **28**(48), 1804915 (2018).
- <sup>143</sup>Z. Li, J. Wu, X. Wang, K. Wang, S. Zhang, W. Xie, and L. Liao, "Controllable fabrication of in-series organic heterostructures for optical waveguide application," *Adv. Opt. Mater.* **7**(19), 1900373 (2019).
- <sup>144</sup>H. Liu, Z. Lu, B. Tang, C. Qu, Z. Zhang, and H. Zhang, "A flexible organic single crystal with plastic-twisting and elastic-bending capabilities and polarization-rotation function," *Angew. Chem.* **132**(31), 13044–13050 (2020).
- <sup>145</sup>M.-P. Zhuo, G.-P. He, X.-D. Wang, and L.-S. Liao, "Organic superstructure microwires with hierarchical spatial organisation," *Nat. Commun.* **12**(1), 2252 (2021).
- <sup>146</sup>M. Rohullah, V. V. Pradeep, J. Ravi, A. V. Kumar, and R. Chandrasekar, "Micromechanically-powered rolling locomotion of a twisted-crystal optical-waveguide cavity as a mobile light polarization rotor," *Angew. Chem.* **134**(21), e202202114 (2022).
- <sup>147</sup>S. Tang, K. Ye, and H. Zhang, "Integrating low-temperature-resistant two-dimensional elastic-bending and reconfigurable plastic-twisting deformations into an organic crystal," *Angew. Chem.* **134**(42), e202210128 (2022).
- <sup>148</sup>Y. Ma, C.-F. Xu, X.-R. Mao, Y. Wu, J. Yang, L.-P. Xu, M.-P. Zhuo, H. Lin, S. Zhuo, and X.-D. Wang, "Oriented self-assembly of hierarchical branch organic crystals for asymmetric photonics," *J. Am. Chem. Soc.* **145**(16), 9285–9291 (2023).
- <sup>149</sup>Y. Yao, Y. S. Zhao, and L. Guan, "Dimension evolution of self-assembled organic microcrystal for laser and polarization-rotation function," *Small* **20**, 2307661 (2024).
- <sup>150</sup>A. V. Kumar, M. Godumala, J. Ravi, and R. Chandrasekar, "A broadband, multiplexed-visible-light-transport in composite flexible-organic-crystal waveguide," *Angew. Chem. Int. Ed.* **61**(48), e202212382 (2022).
- <sup>151</sup>J. W. Reddy, M. Lassiter, and M. Chamanzar, "Parylene photonics: A flexible, broadband optical waveguide platform with integrated micromirrors for biointerfaces," *Microsyst. Nanoeng.* **6**(1), 85 (2020).
- <sup>152</sup>Y. Luo, C. Sun, H. Ma, M. Wei, J. Jian, C. Zhong, J. Li, R. Tang, Z. Chen, K. A. Richardson, H. Lin, and L. Li, "Interlayer slope waveguide coupler for multi-layer chalcogenide photonics," *Photonics* **9**(2), 94 (2022).
- <sup>153</sup>Y. Wang, Y. Zhou, L. Qi, and Y. Zhang, "Soft optical fibers for biomedical and wearable technologies: Current trends and future prospects," *Adv. Funct. Mater.* **35**, 2507712 (2025).
- <sup>154</sup>A. Vinod Kumar and R. Chandrasekar, "Mechanophotonics: Fabrication of a 2 × 2 hybrid directional coupler from flexible organic crystals," *J. Mater. Chem. C* **11**(24), 7995–8001 (2023).
- <sup>155</sup>M. Rohullah, V. K. Avulu, and R. Chandrasekar, "A hybrid organic-crystal-based curved waveguide network for producing, splitting, and transducing multi-color outputs," *Laser Photonics Rev.* **18**(8), 2400020 (2024).
- <sup>156</sup>J. Liu, Q. Wu, X. Sui, Q. Chen, G. Gu, L. Wang, and S. Li, "Research progress in optical neural networks: Theory, applications and developments," *Photonix* **2**(1), 5 (2021).
- <sup>157</sup>B. J. Shastri, A. N. Tait, T. Ferreira de Lima, W. H. P. Pernice, H. Bhaskaran, C. D. Wright, and P. R. Prucnal, "Photonics for artificial intelligence and neuromorphic computing," *Nat. Photonics* **15**(2), 102–114 (2021).
- <sup>158</sup>W. Freude, A. Kotz, H. Kholeif, A. Schwarzenberger, A. Kuzmin, C. Eschenbaum, A. Mertens, S. Sarwar, P. Erk, S. Bräse, and C. Koos, "High-performance modulators employing organic electro-optic materials on the silicon platform," *IEEE J. Select. Top. Quantum Electron.* **30**(4), 1–22 (2024).
- <sup>159</sup>R. Marchetti, C. Lacava, A. Khokhar, X. Chen, I. Cristiani, D. J. Richardson, G. T. Reed, P. Petropoulos, and P. Minzioni, "High-efficiency grating-couplers: Demonstration of a new design strategy," *Sci. Rep.* **7**(1), 16670 (2017).
- <sup>160</sup>X. Zhu, G. Li, X. Wang, Y. Li, R. Davidson, B. E. Little, and S. T. Chu, "Low-loss fiber-to-chip edge coupler for silicon nitride integrated circuits," *Opt. Express* **31**(6), 10525 (2023).
- <sup>161</sup>S. Romero-García, B. Shen, F. Merget, B. Marzban, and J. Witzens, "Alignment tolerant couplers for silicon photonics," *IEEE J. Sel. Top. Quantum Electron.* **21**(6), 765–778 (2015).
- <sup>162</sup>A. Khapre, A. V. Kumar, and R. Chandrasekar, "Powering organic flexible optical waveguides and circuits via focused micro-LEDs for visible light communication," *Laser Photonics Rev.* **19**(1), 2400278 (2025).
- <sup>163</sup>W. D. Sacher, J. C. Mikkelsen, P. Dumais, J. Jiang, D. Goodwill, X. Luo, Y. Huang, Y. Yang, A. Bois, P. G.-Q. Lo, E. Bernier, and J. K. S. Poon, "Tri-layer silicon nitride-on-silicon photonic platform for ultra-low-loss crossings and interlayer transitions," *Opt. Express* **25**(25), 30862–30875 (2017).
- <sup>164</sup>W. D. Sacher, J. C. Mikkelsen, Y. Huang, J. C. C. Mak, Z. Yong, X. Luo, Y. Li, P. Dumais, J. Jiang, D. Goodwill, E. Bernier, P. G.-Q. Lo, and J. K. S. Poon, "Monolithically integrated multilayer silicon nitride-on-silicon waveguide platforms for 3-D photonic circuits and devices," *Proc. IEEE* **106**(12), 2232–2245 (2018).
- <sup>165</sup>N. Lindenmann, G. Balthasar, D. Hillerkuss, R. Schmogrow, M. Jordan, J. Leuthold, W. Freude, and C. Koos, "Photonic wire bonding: A novel concept for chip-scale interconnects," *Opt. Express* **20**(16), 17667 (2012).
- <sup>166</sup>S. Pearson, J. Feng, and A. del Campo, "Lighting the path: Light delivery strategies to activate photoresponsive biomaterials in vivo," *Adv. Funct. Mater.* **31**(50), 2105989 (2021).
- <sup>167</sup>J. Zhang, S. Zhao, Z. Lu, and X. Wang, "Flourishing organic active optical waveguides with diversity and creativity," *Adv. Funct. Mater.* **2025**, e06412.
- <sup>168</sup>D. Bose, M. W. Harrington, A. Isichenko, K. Liu, J. Wang, N. Chauhan, Z. L. Newman, and D. J. Blumenthal, "Anneal-free ultra-low loss silicon nitride integrated photonics," *Light Sci. Appl.* **13**(1), 156 (2024).
- <sup>169</sup>J. F. Bauters, M. J. R. Heck, D. John, D. Dai, M.-C. Tien, J. S. Barton, A. Leinse, R. G. Heideman, D. J. Blumenthal, and J. E. Bowers, "Ultra-low-loss high-aspect-ratio Si<sub>3</sub>N<sub>4</sub> waveguides," *Opt. Express* **19**(4), 3163–3174 (2011).

- <sup>170</sup>Y.-T. Yang and C.-M. Hung, "Heterogeneous integration in co-packaged optics," *IEEE J. Emerg. Sel. Top. Circuits Syst.* **15**(3), 427–437 (2025).
- <sup>171</sup>M. Rohullah, M. Chosenyah, A. V. Kumar, and R. Chandrasekar, "Cornu-spiral-like organic crystal waveguide providing discriminatory optical pathway for smart organic photonic circuit," *Small* **21**(8), 2407498 (2025).
- <sup>172</sup>J. J. Griebel, S. Namnabat, E. T. Kim, R. Himmelhuber, D. H. Moronta, W. J. Chung, A. G. Simmonds, K.-J. Kim, J. van der Laan, N. A. Nguyen, E. L. Dereniak, M. E. Mackay, K. Char, R. S. Glass, R. A. Norwood, and J. Pyun, "New infrared transmitting material via inverse vulcanization of elemental sulfur to prepare high refractive index polymers," *Adv. Mater.* **26**(19), 3014–3018 (2014).
- <sup>173</sup>D. McCloskey and J. F. Donegan, "Silicon nitride microdisks in the visible range," in *Proceedings of the 2011 13th International Conference on Transparent Optical Networks* (IEEE, 2011), pp. 1–4.
- <sup>174</sup>C. G. H. Roeloffzen, M. Hoekman, E. J. Klein, L. S. Wevers, R. B. Timens, D. Marchenko, D. Gekus, R. Dekker, A. Alippi, R. Grootjans, A. van Rees, R. M. Oldenbeuving, J. P. Epping, R. G. Heideman, K. Wörhoff, A. Leinse, D. Geuzebroek, E. Schreuder, P. W. L. van Dijk, I. Visscher, C. Taddei, Y. Fan, C. Taballione, Y. Liu, D. Marpaung, L. Zhuang, M. Benelajla, and K.-J. Boller, "Low-loss Si<sub>3</sub>N<sub>4</sub> TriPleX optical waveguides: Technology and applications overview," *IEEE J. Select. Top. Quantum Electron.* **24**(4), 1–21 (2018).
- <sup>175</sup>T. Ishigure, S. Yoshida, K. Yasuhara, and D. Suganuma, "Low-loss single-mode polymer optical waveguide at 1550-nm wavelength compatible with silicon photonics," in *Proceedings of the 2015 IEEE 65th Electronic Components and Technology Conference (ECTC)* (IEEE, 2015), pp. 768–774.
- <sup>176</sup>L. Yu. Beliaev, E. Shkondin, A. V. Lavrinenko, and O. Takayama, "Optical, structural and composition properties of silicon nitride films deposited by reactive radio-frequency sputtering, low pressure and plasma-enhanced chemical vapor deposition," *Thin Solid Films* **763**, 139568 (2022).
- <sup>177</sup>B. Liu, Q. Di, W. Liu, C. Wang, Y. Wang, and H. Zhang, "Red-emissive organic crystals of a single-benzene molecule: Elastically bendable and flexible optical waveguide," *J. Phys. Chem. Lett.* **10**(7), 1437–1442 (2019).
- <sup>178</sup>S. Tang, K. Ye, P. Commings, L. Li, P. Naumov, and H. Zhang, "Organic crystalline optical waveguides that remain elastic from −196 to ≈200 °C," *Adv. Opt. Mater.* **11**(13), 2200627 (2023).
- <sup>179</sup>P. Reddy, S. Washiyama, F. Kaess, M. Hayden Breckenridge, L. H. Hernandez-Balderrama, B. B. Haidet, D. Alden, A. Franke, B. Sarkar, E. Kohn, R. Collazo, and Z. Sitar, "High temperature and low pressure chemical vapor deposition of silicon nitride on AlGaIn: Band offsets and passivation studies," *J. Appl. Phys.* **119**(14), 145702 (2016).
- <sup>180</sup>J. Yota, J. Handers, and A. A. Saleh, "A comparative study on inductively-coupled plasma high-density plasma, plasma-enhanced, and low pressure chemical vapor deposition silicon nitride films," *J. Vac. Sci. Technol. A* **18**(2), 372–376 (2000).
- <sup>181</sup>E.-S. Lee, K.-W. Chun, J. Jin, and M.-C. Oh, "Enhancement of the thermo-optic phase modulation efficiency in silicon nitride waveguides by incorporating an embedded strip within a planar polymer waveguide," *Opt. Express* **33**(3), 5099–5107 (2025).
- <sup>182</sup>L. Lan, L. Li, P. Naumov, and H. Zhang, "Flexible organic crystals for dynamic optical transmission," *Chem. Mater.* **35**(18), 7363–7385 (2023).
- <sup>183</sup>J. P. Epping, M. Hoekman, R. Mateman, A. Leinse, R. G. Heideman, A. van Rees, P. J. M. van der Slot, C. J. Lee, and K.-J. Boller, "High confinement, high yield Si<sub>3</sub>N<sub>4</sub> waveguides for nonlinear optical applications," *Opt. Express* **23**(2), 642–648 (2015).
- <sup>184</sup>J. Liu, G. Huang, R. N. Wang, J. He, A. S. Raja, T. Liu, N. J. Engelsen, and T. J. Kippenberg, "High-yield, wafer-scale fabrication of ultralow-loss, dispersion-engineered silicon nitride photonic circuits," *Nat. Commun.* **12**(1), 2236 (2021).
- <sup>185</sup>M. Weis, "Organic semiconducting polymers in photonic devices: From fundamental properties to emerging applications," *Appl. Sci.* **15**(7), 4028 (2025).
- <sup>186</sup>B. Stern, X. Ji, Y. Okawachi, A. L. Gaeta, and M. Lipson, "Battery-operated integrated frequency comb generator," *Nature* **562**(7727), 401–405 (2018).
- <sup>187</sup>Z. Ye, H. Jia, Z. Huang, C. Shen, J. Long, B. Shi, Y.-H. Luo, L. Gao, W. Sun, H. Guo, J. He, and J. Liu, "Foundry manufacturing of tight-confinement, dispersion-engineered, ultralow-loss silicon nitride photonic integrated circuits," *Photonics Res.* **11**(4), 558–568 (2023).